RESEARCH ARTICLE

Somatic Superenhancer Duplications and Hotspot Mutations Lead to Oncogenic Activation of the KLF5 Transcription Factor

Xiaoyang Zhang[1,2], Peter S. Choi[1,2], Joshua M. Francis[1,2], Galen F. Gao[2], Joshua D. Campbell[1,2], Aruna Ramachandran[1,2], Yoichiro Mitsuishi[1,2], Gavin Ha[1,2], Juliann Shih[2], Francisca Vazquez[2], Aviad Tsherniak[2], Alison M. Taylor[1,2], Jin Zhou[1], Zhong Wu[1], Ashton C. Berger[2], Marios Giannakis[1,2], William C. Hahn[1,2,3], Andrew D. Cherniack[1,2], and Matthew Meyerson[1,2,3,4]

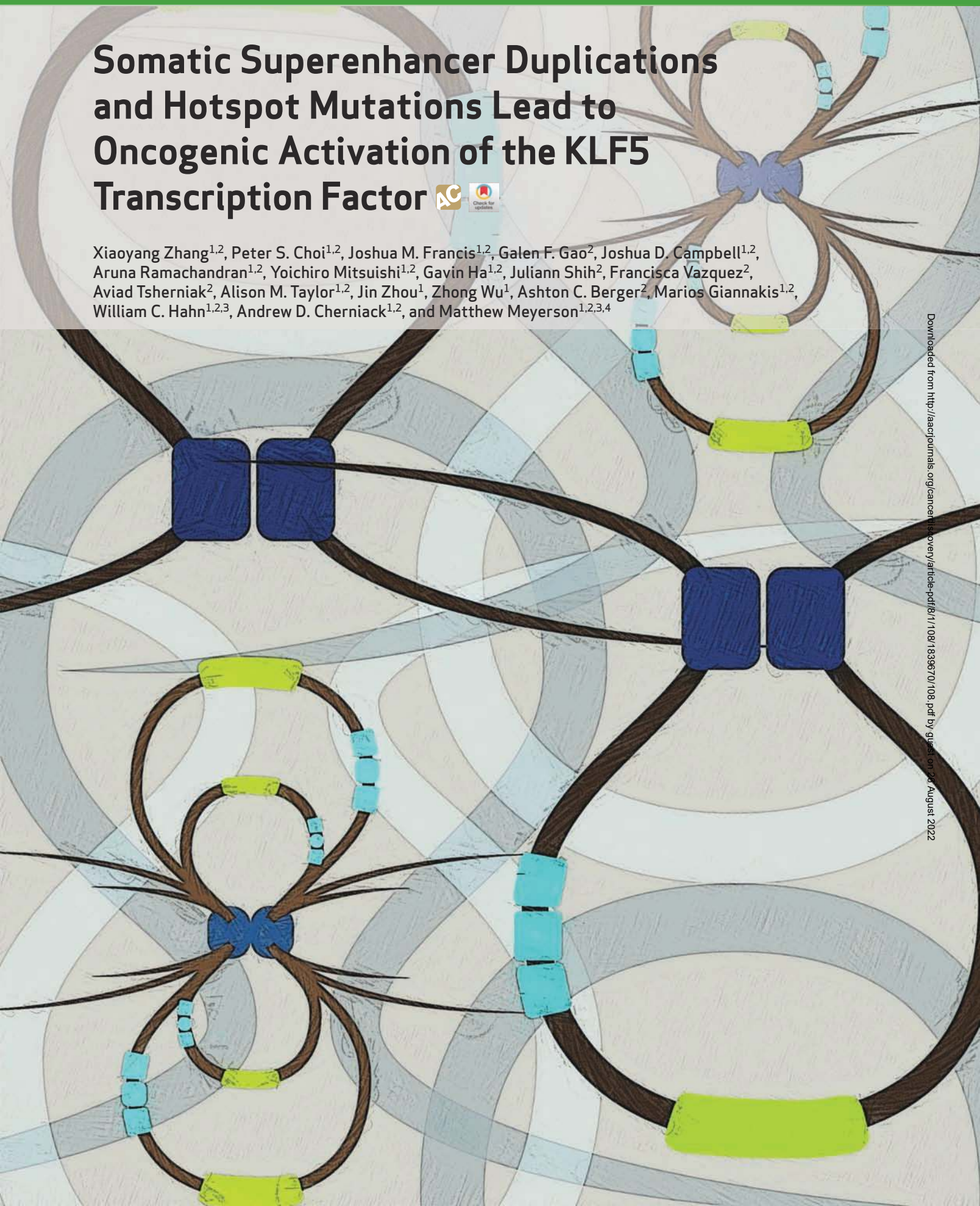

ABSTRACT The Krüppel-like family of transcription factors plays critical roles in human development and is associated with cancer pathogenesis. Krüppel-like factor 5 gene (*KLF5*) has been shown to promote cancer cell proliferation and tumorigenesis and to be genomically amplified in cancer cells. We recently reported that the *KLF5* gene is also subject to other types of somatic coding and noncoding genomic alterations in diverse cancer types. Here, we show that these alterations activate KLF5 by three distinct mechanisms: (i) Focal amplification of superenhancers activates *KLF5* expression in squamous cell carcinomas; (ii) Missense mutations disrupt KLF5–FBXW7 interactions to increase KLF5 protein stability in colorectal cancer; (iii) Cancer type–specific hotspot mutations within a zinc-finger DNA binding domain of KLF5 change its DNA binding specificity and reshape cellular transcription. Utilizing data from CRISPR/Cas9 gene knockout screening, we reveal that cancer cells with *KLF5* overexpression are dependent on KLF5 for their proliferation, suggesting KLF5 as a putative therapeutic target.

SIGNIFICANCE: Our observations, together with previous studies that identified oncogenic properties of KLF5, establish the importance of KLF5 activation in human cancers, delineate the varied genomic mechanisms underlying this occurrence, and nominate KLF5 as a putative target for therapeutic intervention in cancer. *Cancer Discov; 8(1); 108–25. ©2017 AACR.*

INTRODUCTION

Genomic alterations during tumorigenesis can lead to the activation of oncogenic transcription factors, resulting in aberrant gene regulation throughout the genome. For example, somatic structural variations such as copy-number amplifications increase gene dosage of *MYC, MYCN, AR, MITF,* and *SOX2* and upregulate their expression (1–6); chromosomal translocations can place regulatory elements such as enhancers or superenhancers adjacent to oncogenes and activate their expression, as observed with *MYC, MYB,* and *ERG* (7–12); whereas amplification of noncoding superenhancers is known to activate *MYC* (13–15). In addition, somatic single-nucleotide variants (SNV) can activate oncogenic transcription factors; for example, missense mutations in the degron domains of NFE2L2 stabilize the protein by preventing its binding to the E3 ubiquitin ligase KEAP1 (16, 17). In noncoding regions, somatic mutations are known to increase the activity of distal enhancers or superenhancers to activate *ESR1* and *TAL1* expression (18, 19).

We and others have recently obtained genomic evidence that the Krüppel-like factor 5 gene (*KLF5*) could act as an oncogene. Previous studies have reported copy-number amplification of broad regions on chromosome 13q harboring the *KLF5* gene in gastric and salivary gland tumors (20, 21). We identified noncoding superenhancers that are focally amplified ~300 kb 3′ to the *KLF5* gene in head and neck squamous cell carcinomas (HNSC), which correlates with *KLF5* overexpression (15). In addition, we have identified recurrent missense mutations in a zinc-finger (ZNF) DNA binding domain of *KLF5* in lung adenocarcinomas, lung squamous cell carcinomas (LUSC), and in a phospho-degron domain of *KLF5* in colorectal carcinomas (22, 23).

Krüppel-like transcription factors (KLF) play important roles in development and disease. KLF4 is one of the four key transcription factors required for maintaining the pluripotency of embryonic stem cells (24). In epithelial cells, KLF4 inhibits cell-cycle progression and is highly expressed in terminally differentiated cells (25). In contrast, KLF5 promotes cell proliferation and is highly expressed in actively dividing cells (26). Previous studies have suggested that KLF5 has oncogenic properties. In addition to its role as a positive regulator of cancer cell proliferation (27, 28), overexpression of KLF5 has been reported to promote tumorigenesis of multiple cancer types, including intestinal, bladder, and gastric cancers (29–31). KLF5 has also been linked to intestinal tumorigenesis at the stem-cell level (32, 33). Furthermore, KLF5 overexpression is also a prognostic marker for worse survival of patients with breast cancer (34).

In light of this previous literature and our recent genomic data, we decided to systematically investigate noncoding and coding genomic alterations related to the *KLF5* gene and their transcriptional and phenotypic consequences. We performed functional analysis of each of these genomic alterations to understand how they contribute to oncogenic activation of KLF5 and their effects on *KLF5* gene expression, protein stability, and protein function. Our results highlight a variety of somatic genome alterations that converge to enhance the levels and activity of KLF5, and thereby to reshape cellular transcriptional programs and promote cancer cell proliferation.

[1]Department of Medical Oncology, Dana-Farber Cancer Institute, Boston, Massachusetts. [2]Cancer Program, Broad Institute of Harvard and MIT, Cambridge, Massachusetts. [3]Center for Cancer Genome Discovery, Dana-Farber Cancer Institute, Boston, Massachusetts. [4]Department of Pathology, Harvard Medical School, Boston, Massachusetts.

Note: Supplementary data for this article are available at Cancer Discovery Online (http://cancerdiscovery.aacrjournals.org/).

Current address for J.M. Francis: Gritstone Oncology, Cambridge, Massachusetts; current address for J.D. Campbell: School of Medicine, Boston University, Boston, Massachusetts.

Corresponding Author: Matthew Meyerson, Dana-Farber Cancer Institute, Boston, MA 02215. Phone: 617-632-4768; Fax: 617-582-7880; E-mail: matthew_meyerson@dfci.harvard.edu

doi: 10.1158/2159-8290.CD-17-0532

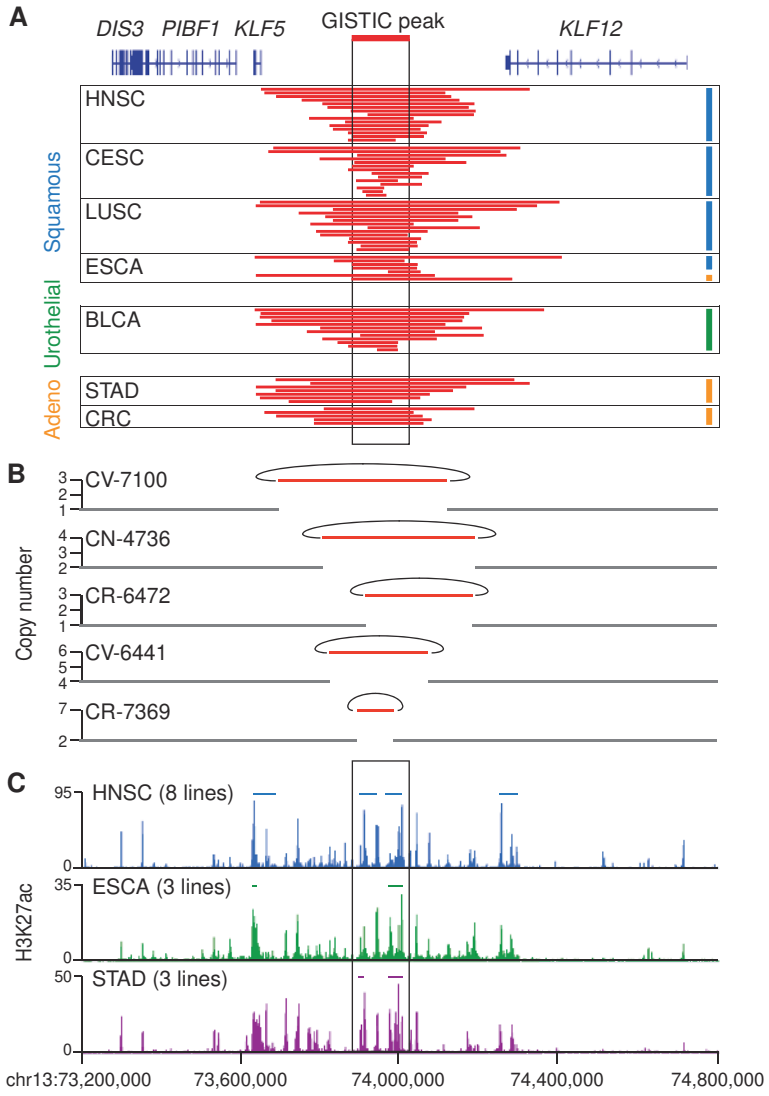

Figure 1. Superenhancers near the *KLF5* gene are focally amplified in diverse cancer types. **A,** Copy-number profile of the 13q22.1 noncoding region from HNSC, CESC, LUSC, ESCA, BLCA, STAD, and CRC. The copy-number peak, defined by statistical analysis with GISTIC (2, 109), in HNSC is highlighted. Color code is based on lineage types: squamous cell carcinomas, blue; urothelial carcinomas, green; adenocarcinomas, orange. **B,** DNA rearrangement analysis of the amplified noncoding region, using whole-genome sequencing data of head and neck squamous carcinoma samples from TCGA and the LUMPY program (37), demonstrates tandem duplications, as indicated by the curves. **C,** The merged ChIP-seq signal of the enhancer marker H3K27ac from cell lines representing HNSC, ESCA, and STAD. Superenhancers, indicated by thin bars, are called by the ROSE pipeline (39–41) based on the H3K27ac signal enrichment. BLCA, bladder carcinoma; CESC, cervical squamous cell carcinoma; CRC, colorectal adenocarcinoma; ESCA, esophageal carcinoma; GISTIC, genomic identification of significant targets in cancer; STAD, stomach adenocarcinoma; TCGA, The Cancer Genome Atlas.

RESULTS

Focal Amplification of Noncoding Superenhancers Activates *KLF5* Expression

To define the prevalence of *KLF5* superenhancer amplification across cancers, we examined SNP array–based copy-number data targeting the ~600 kb intergenic region between *KLF5* and *KLF12* on chromosome segment 13q22.1 across 10,844 samples from 33 cancer types included in The Cancer Genome Atlas (TCGA). We discovered recurrent amplifications of this noncoding region in six other cancer types beyond HNSC (15/522), including esophageal carcinomas (ESCA; 7/184), cervical squamous cell carcinomas (CESC; 14/295), LUSC (14/501), bladder carcinomas (BLCA; 12/408), stomach adenocarcinomas (STAD; 7/441), and colorectal adenocarcinomas (5/615; Fig. 1A). Consistent with these observations, an analysis of SNP array–based copy-number data from 1,043 cancer cell lines within the Broad Institute's Cancer Cell Line Encyclopedia (CCLE) project (35) identified focal amplification of this noncoding region in 12 cell lines, from the 7 cancer types reported above (Supplementary Fig. S1A). Examination of the copy-number profile from TCGA normal tissues (n = 11,813) found no evidence of amplifications of the *KLF5* noncoding region.

To investigate the molecular basis for amplification of the *KLF5/KLF12* intervening region, we analyzed whole-genome sequencing (WGS) data (36) for six HNSC samples bearing this amplification. DNA rearrangement analysis of the WGS data, using the structural variant calling program LUMPY (37), validated the focal amplification events in five of the six samples and revealed that they occur in a tandem duplication pattern (Fig. 1B). Correspondingly, DNA rearrangement analysis of WGS data from three cancer cell lines with this amplification, from disparate cancer types, revealed tandem duplication of the noncoding region (Supplementary Fig. S1B). Chromatin immunoprecipitation sequencing (ChIP-seq) in cell lines representing eight HNSC, three ESCA, and three STAD showed similar profiles of histone H3 lysine 27 acetylation (H3K27ac), a marker of enhancer elements (38), at the *KLF5* noncoding locus (Fig. 1C; Supplementary Fig. S2A). Distinct from typical enhancers, superenhancers are large clusters of enhancers that are associated with the

activation of cell identity genes and cancer-related genes (39–41). We analyzed the H3K27ac ChIP-seq data using the ROSE pipeline (39–41) and identified several superenhancers in the amplified region (Fig. 1C, rectangle), one in ESCA cells and two in HNSC and STAD cells (Fig. 1C, indicated by bars within the rectangle). Taken together, these data suggest that focal amplification of noncoding superenhancers near the *KLF5* gene is a recurrent event in multiple cancer types, particularly squamous cell carcinomas.

The amplified superenhancers are located in a ~600 kb noncoding region flanked by *KLF5* on the centromeric side and *KLF12* on the telomeric side (Fig. 1A). Enhancers regulate gene expression through physical interaction with gene promoters (42–44), and these interactions are restricted by topologically associating domains (TAD), chromatin "neighborhoods" that are highly conserved across tissue types (45–51). Utilizing publicly available Hi-C data from IMR90 lung fibroblast cells that measure physical interactions between chromatin regions and define TADs in the genome (49), we found that the amplified superenhancers lie within the same TAD (small TAD, chr13:73,570,000–74,290,000; large TAD, chr13:73,350,000–74,290,000) as the promoter region and gene body of *KLF5,* but not the promoter or complete gene body of *KLF12*, suggesting that *KLF5* is the candidate target gene (Fig. 2A and B). Indeed, a recent study in a stomach adenocarcinoma cell line identified significant chromatin interaction between the superenhancer region and the *KLF5* (but not the *KLF12*) promoter, using circularized chromosome conformation capture (4C) assays (52). We performed chromosome conformation capture (3C) assays and validated the physical interaction between the superenhancer region and the *KLF5* promoter in cells with (BICR31) or without (BICR6) the superenhancer duplication (Fig. 2C, upper panel). Because most of the 13q22.1 superenhancer amplifications were observed in squamous cell carcinomas (Fig. 1), we analyzed RNA-sequencing (RNA-seq) data from TCGA squamous cell carcinoma samples, including head and neck, cervical, lung, and esophageal squamous carcinoma samples (16, 36, 53–55). We found *KLF5* expression to be greater than *KLF12* expression across all of these cancers. In addition, we observed a mean of 39.7% statistically significant elevation in expression (*t* test: $P < 0.0001$) of *KLF5* in cancers harboring the superenhancer amplifications, compared with tumors without the amplifications, but no significant increase of *KLF12* expression (Supplementary Fig. S2B).

A Combination of Three Individual Enhancers within the Amplified Superenhancers Drives *KLF5* Overexpression

We selected the HNSC cell line BICR31, in which the *KLF5* superenhancers are focally amplified (Supplementary Fig. S1A), as a model system for detailed functional studies. ChIP-seq assays of p300, a marker for active enhancers (56), identified four strong individual enhancer elements in the superenhancers in BICR31 cells (Fig. 2B). We applied the CRISPR-mediated repression system (15, 57, 58), which uses a short guide RNA (sgRNA) to recruit inactivated Cas9 (dCas9) fused to the Krüppel-associated box (KRAB) transcriptional repressor domain (KRAB–dCas9), to repress the e1–e4 enhancers, individually. Repression of each of the individual enhancers e1, e3, or e4 alone (but not e2) resulted in a modest yet significant reduction (20–34%) in *KLF5* expression (Fig. 2D). In agreement, 3C assays detected stronger physical interaction between the *KLF5* promoter and the e1, e3, and e4 enhancers, compared with the e2 enhancer (Fig. 2C, lower panel). Repression of the individual enhancers did not affect expression of *KLF12*, present outside the TAD domain, or of

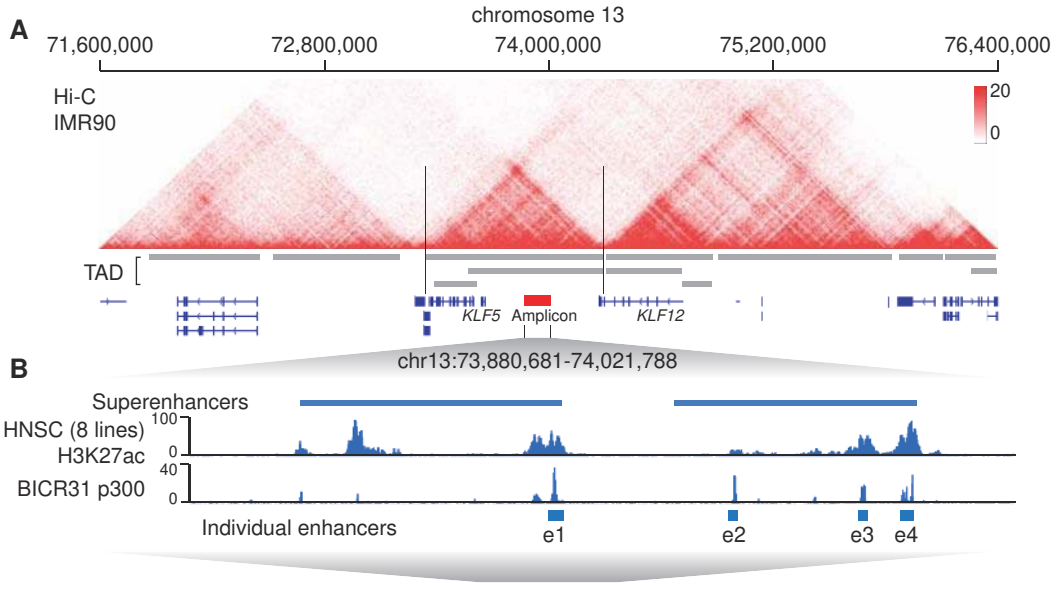

Figure 2. The focally amplified superenhancers activate *KLF5* expression. **A,** Chromatin interaction, as measured by Hi-C in the lung fibroblast cell line IMR90, is presented in the *KLF5* locus. The TADs are indicated as grey bars. **B,** Four individual enhancers, e1–e4, within the superenhancers are defined by p300 ChIP-seq signal from the HNSC cell line BICR31. (*continued on next page*)

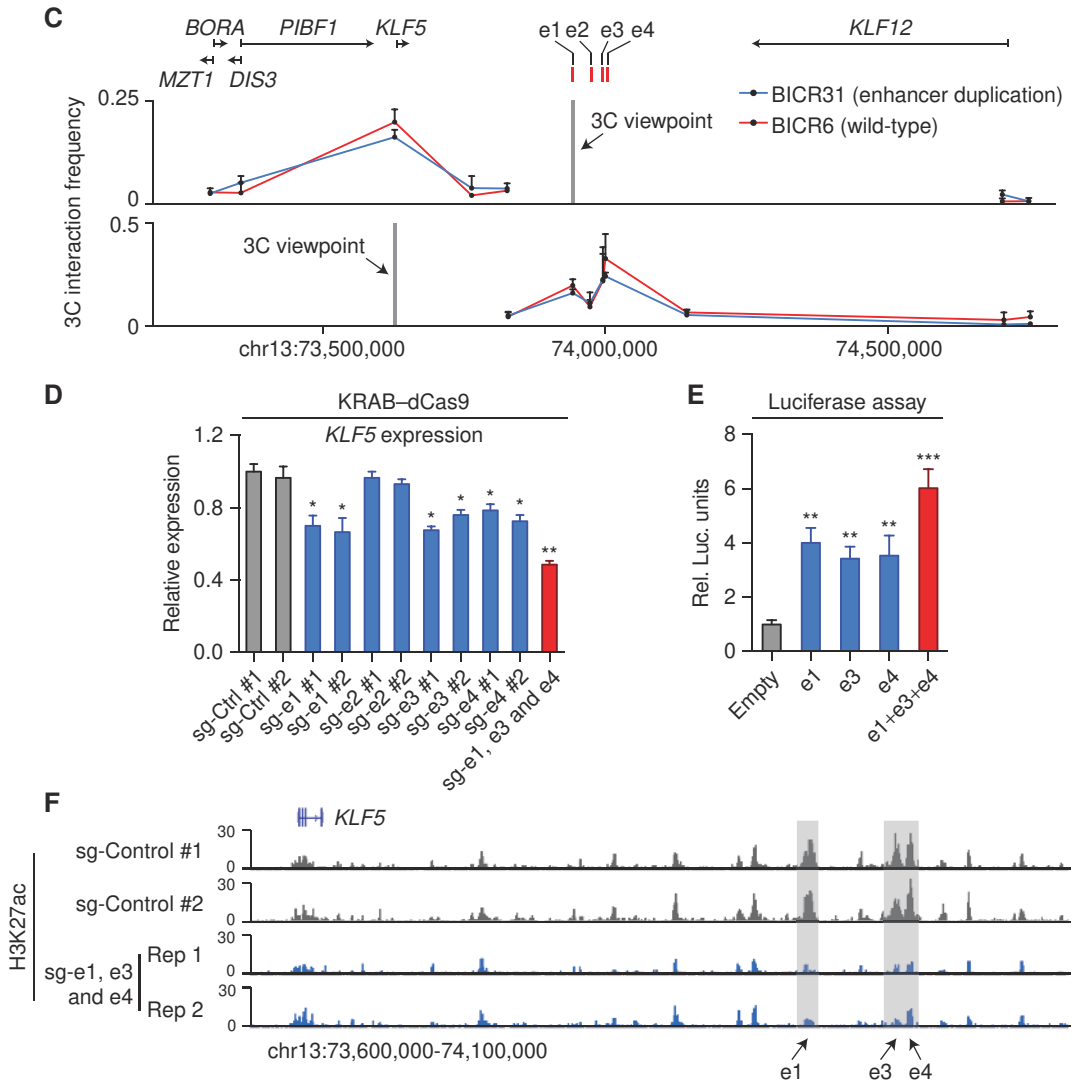

Figure 2. ***(Continued)*** **C,** Chromatin interaction, as measured by 3C-qPCR, between the e1 enhancer and promoters of surrounding genes including *BORA*, *DIS3*, *PIBF1*, *KLF5*, and *KLF12* (top), and between the *KLF5* promoter and the four individual enhancers e1-e4 of the superenhancer region (bottom) in BICR31 and BICR6 cells ($n = 2$). The interaction frequency between the *KLF5* promoter and the e1 enhancer in each panel is represented by the same data. 3C viewpoints are indicated as gray lines. Error bars, SD. **D,** The expression level of *KLF5* after KRAB-dCas9-mediated repression of the individual enhancers e1–e4 in BICR31 cells ($n = 2$). sg-Ctrl #1 and #2: control sgRNAs that are predicted to not recognize any genomic regions. Two separate sgRNAs are applied for each enhancer. Multiplexed repression of the e1, e3, and e4 enhancers (sg-e1 #1, sg-e3 #1, and sg-e4 #1) is highlighted in red. The expression level is normalized to the control (sg-Ctrl #1). Error bars, SD. *P* values were derived from *t* tests: *, $P \le 0.05$; **, $P \le 0.01$. **E,** Luciferase reporter assays ($n = 3$) measuring the activity of the individual enhancers e1, e3, and e4, and the combinatorial activity of the three enhancers in driving the luciferase expression in BICR31 cells. Luciferase signal is normalized to the empty luciferase reporter construct. Error bars, SD. *P* values were derived from *t* tests: **, $P \le 0.01$; ***, $P \le 0.001$. **F,** ChIP-seq profile of H3K27ac in BICR31 cells with and without KRAB-dCas9-mediated multiplexed repression of the three enhancers e1, e3, and e4. The targeted regions are highlighted as gray boxes.

PIBF1 or *DIS3* within the same large TAD domain (Supplementary Fig. S3).

We next sought to interrogate the combinatorial effects of these enhancers. Transfection of a luciferase reporter construct containing all three enhancers gave rise to significantly higher luciferase expression than reporter constructs carrying an individual enhancer, suggesting a joint effect of the three enhancers in activating gene expression (Fig. 2E). Furthermore, multiplexed repression of the e1, e3, and e4 enhancers by KRAB–dCas9 resulted in a marked decrease in overall enhancer activity, as observed by a loss of H3K27ac enrichment at the targeted regions (Fig. 2F), along with a strong reduction (~51%) in *KLF5* expression and a modest reduction (~25%) in *PIBF1* and *DIS3* expression (Fig. 2D; Supplementary Fig. S3). These data reveal that the e1, e3, and e4 enhancers exert a combinatorial effect on gene activation, with *KLF5* as the primary gene target.

KLF5 Activates Cell Identity Genes and Cancer-Related Genes in Squamous Cell Carcinomas

To assess the gene regulatory functions of KLF5 in squamous cell carcinomas, we performed ChIP-seq assays using

an antibody against endogenous KLF5 in the head and neck squamous carcinoma cell line BICR31. We observed that 20.7% of KLF5 binding sites occurred at promoter regions (promoter enrichment: Fisher exact test, $P = 10^{-322}$), with 73.3% distributed across intergenic or intronic regions (Supplementary Fig. S4A). Motif analysis of the KLF5 binding sites, using the SeqPos tool (59), revealed that KLF5 recognizes the same DNA binding motif (GGGG T/C GGGGC) as other KLFs and Specificity proteins (Sp; Fig. 3A; refs. 60, 61). We also identified DNA binding motifs for other transcription factors, including ETS1, ERG, AP1, and TP63, suggesting their involvement in the oncogenic role of KLF5 (Supplementary Fig. S4B). Further analysis revealed that the KLF5 binding sites are enriched for p300 binding and H3K27ac modifications, indicating that KLF5 binding is associated with active regulatory elements (Fig. 3B). Our results are consistent with previous reports that the transactivation function of KLF5 depends on its interaction with the CBP/p300 coactivator complex (62). Annotating KLF5 binding sites in more detail, we observed that KLF5 binding sites are more prevalent in superenhancers than in typical enhancers. Indeed, individual active enhancers (as defined by p300 binding in BICR31 cells) are more likely to be bound by KLF5 (~33%) when present in superenhancers rather than in typical enhancers (~22%; Fig. 3C).

To investigate the transcriptional impact of KLF5 expression, we conducted RNA-seq assays in BICR31 cells with and without siRNA-mediated silencing of *KLF5* (Supplementary Fig. S5A). We integrated the RNA-seq and KLF5 ChIP-seq results with the binding and expression target analysis (BETA) pipeline (63), which first assigns each gene in the genome a KLF5 regulatory potential score based on two criteria: (i) the number of KLF5 binding sites within ±50 kb of the transcription start site (TSS) for each queried gene, and (ii) the distance between these KLF5 binding sites and the TSS. We then used BETA to interrogate the impact of perturbing KLF5 abundance on expression of each of these genes. This analysis revealed that KLF5 activates the expression of genes with higher KLF5 regulatory potential scores more often than it represses the expression of such genes (Fig. 3D; Kolmogorov–Smirnov test, $P = 2.3 \times 10^{-8}$), suggesting that KLF5 mainly acts as a transcriptional activator. We also detected a modest yet significant reduction (~20% in average, *t* test: $P < 0.001$) in the H3K27ac level surrounding KLF5 binding sites that are nearest to KLF5-activated genes (Supplementary Fig. S6). We observe that KLF5 activates squamous cell identity genes such as *KRT5, KRT8, KRT6A, KRT13, LAMA3, LAMB3*, and *LAMC2,* and cancer-related genes such as *ID1, CCND1, TP63, DEK, WNT10A, PDGFA*, and *PDGFB* (Fig. 3E; Supplementary Fig. S5B). To validate this observation, we targeted the KLF5 binding sites surrounding *ID1* by the KRAB–dCas9 repressor complex and found a significant decrease in *ID1* expression, demonstrating a direct role of KLF5 binding in activating *ID1* (Fig. 3F).

Hotspot Mutations in a Phospho-Degron Domain Increase KLF5 Protein Stability

In addition to focal amplifications of noncoding superenhancers, mutations within the *KLF5* gene are also frequently found in cancer (22, 23). We examined the mutation profile of KLF5 in >11,000 tumor samples from the TCGA project (64–69) as well as 619 colorectal cancer samples from 2 prospective cohort studies (23). This analysis confirmed the presence of two mutation hotspots in *KLF5*: one within a phospho-degron domain and the other within a DNA binding domain (Fig. 4A; Supplementary Fig. S7; see Methods section for additional details on mutation hotspot identification). Three FBXW7 (also known as CDC4) phospho-degron domains (CPD) have been identified in KLF5 (70), which have been shown, when phosphorylated, to bind the E3 ubiquitin ligase FBXW7, leading to the ubiquitination and degradation of KLF5 (70). Our analysis revealed that the second CPD (amino acids 301–307: PPSPPSS) is a target of missense mutations, seen mainly in colorectal cancer (7/619; $P = 5.65 \times 10^{-30}$; data from ref. 23; Fig. 4A; Supplementary Fig. S7A). A previous study has shown that the P301S mutation inhibits the interaction between FBXW7 and KLF5 and increases the protein stability of KLF5 (71). To assess if this is a common mechanism for the hotspot mutations, we included two other mutations, S303P and P304A, and performed a cycloheximide (CHX) chase assay in the colorectal cancer cell line HCT116 to measure their effects on KLF5 protein stability. We found that the three tested mutations significantly reduced degradation of KLF5 to a similar extent, compared with wild-type (WT) KLF5 (Fig. 4B). Coimmunoprecipitation assays confirmed that the mutations impaired the interaction of KLF5 with FBXW7 (Fig. 4C).

Notably, the *FBXW7* gene is also significantly mutated in colorectal cancers (~13%), with recurrent mutations enriched in the WD40 repeat domains required for interaction with its substrates (refs. 72, 73; Supplementary Fig. S8A). None of the colorectal cancer samples harboring *KLF5* hotspot mutations had mutations in *FBXW7* (Supplementary Fig. S8B). We tested three of the most recurrent *FBXW7* missense mutations, R465C, R465H, and R505C, and found that they indeed impaired the interaction of FBXW7 with KLF5 (Fig. 4D). Although overexpression of WT FBXW7 in HCT116 cells decreased the protein level of KLF5, the FBXW7 mutants showed an opposite effect (Fig. 4E), consistent with previous findings that FBXW7 mutations have dominant negative effects (74, 75). Taken together, we found here that hotspot mutations within either the KLF5 CPD domain or the FBXW7 WD40 repeat domains act to stabilize KLF5 levels by preventing its binding to FBXW7.

Hotspot Mutations in a DNA Binding Domain of *KLF5* Alter Its DNA Binding Specificity

An additional hotspot mutation is found in *KLF5* ($P = 4.26 \times 10^{-63}$; TCGA pan-cancer dataset; ref. 64) within the second of three DNA-binding ZNF domains that are highly conserved within KLF family members (61), with significant recurrent mutations at the codons for D418 and E419 in lung adenocarcinomas (2/502) and LUSC (7/464; ref. 22; Fig. 5A; Supplementary Fig. S7B). Pan-cancer analysis identified additional hotspot mutations at these positions in CESC (6/272), BLCA (5/398), and STAD (1/383; Fig. 5A). Interestingly, these mutations are cancer type–specific. For example, the E419K mutation occurs predominantly in CESC whereas the E419Q mutation is observed only in lung cancers (Fig. 5A).

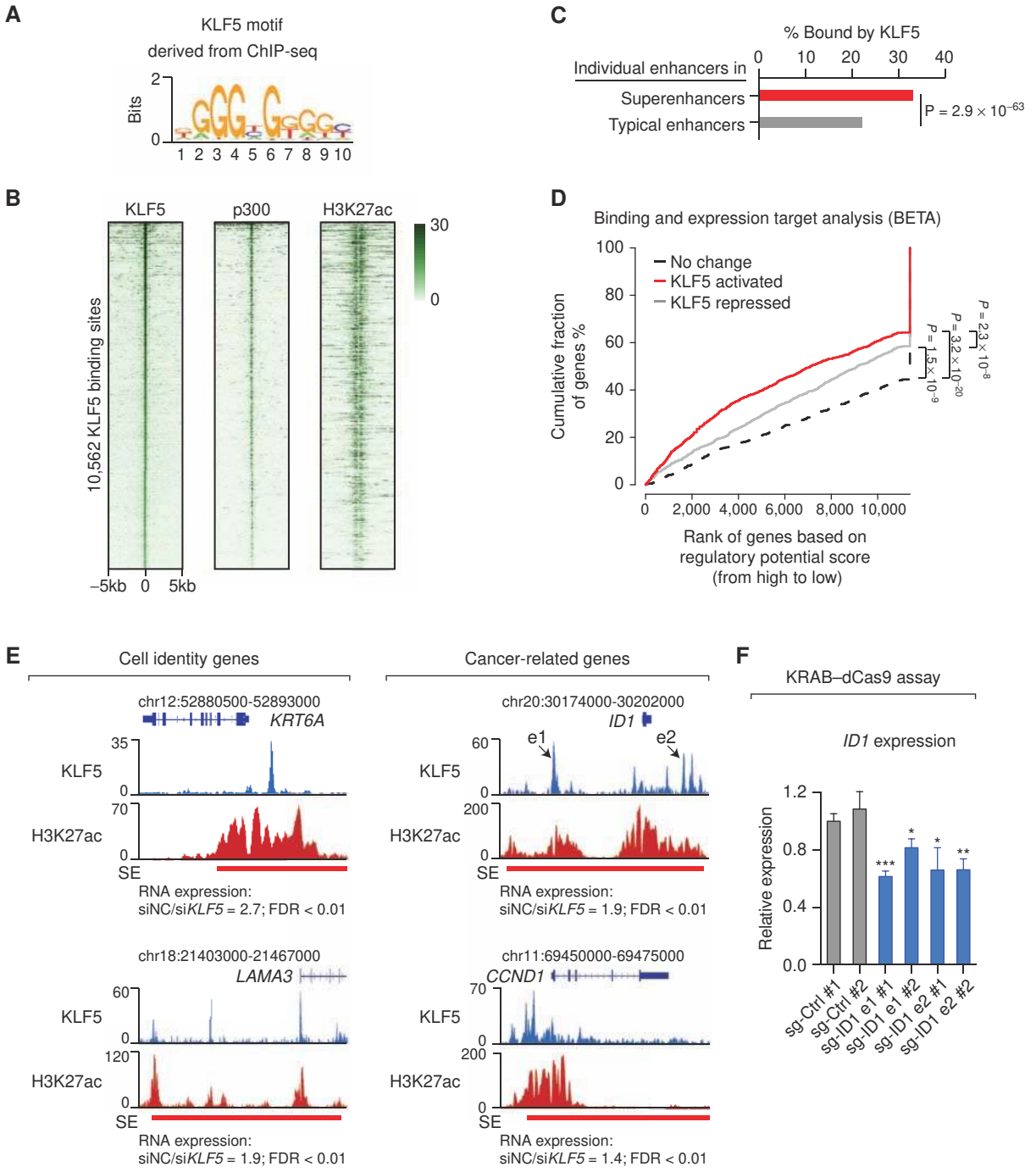

Figure 3. *KLF5* activates cell identity genes and cancer-related genes in HNSC cells. **A,** Predicted DNA binding motif of KLF5 derived from the DNA binding pattern of endogenous KLF5, detected by ChIP-seq. **B,** Enrichment of p300 binding and H3K27ac marks centered around KLF5 binding sites ($n = 10,562$) in BICR31 cells. **C,** Percentage of individual enhancers, as defined by p300 binding, bound by KLF5 in typical and superenhancers called from H3K27ac ChIP-seq signals merged from eight HNSC cell lines. *P* value was derived from a Fisher exact test. **D,** BETA predicting the activating and repressive function of KLF5. The KLF5 ChIP-seq binding sites are integrated with the expression data from the RNA-seq profile in BICR31 cells with and without siRNA-mediated *KLF5* silencing ($n = 3$). More details are described in the Methods section. The red, gray, and black lines represent genes activated, repressed, or unaffected by KLF5, respectively. Percentage of genes is cumulated by the rank of genes based on their regulatory potential scores. *P* values were derived from Kolmogorov–Smirnov tests. **E,** Examples of superenhancer-driven cell identity genes (left) and cancer-related genes (right) activated by KLF5. ChIP-seq profile of KLF5 binding (in BICR31) and H3K27ac marks (merged from eight HNSC cell lines), and distribution of the identified superenhancers (SE). Fold change in the expression level of KLF5-target genes in BICR31 cells with and without siRNA-mediated *KLF5* silencing, as measured by RNA-seq ($n = 3$), is indicated underneath. **F,** KRAB-dCas9 mediated repression of the e1 and e2 enhancers adjacent to *ID1* (indicated in **E**; $n = 3$) reduced *ID1* expression. Expression levels are normalized to the control (sg-Ctrl #1). Error bars, SD. *P* values were derived from *t* tests: *, $P \le 0.05$; **, $P \le 0.01$; ***, $P \le 0.001$.

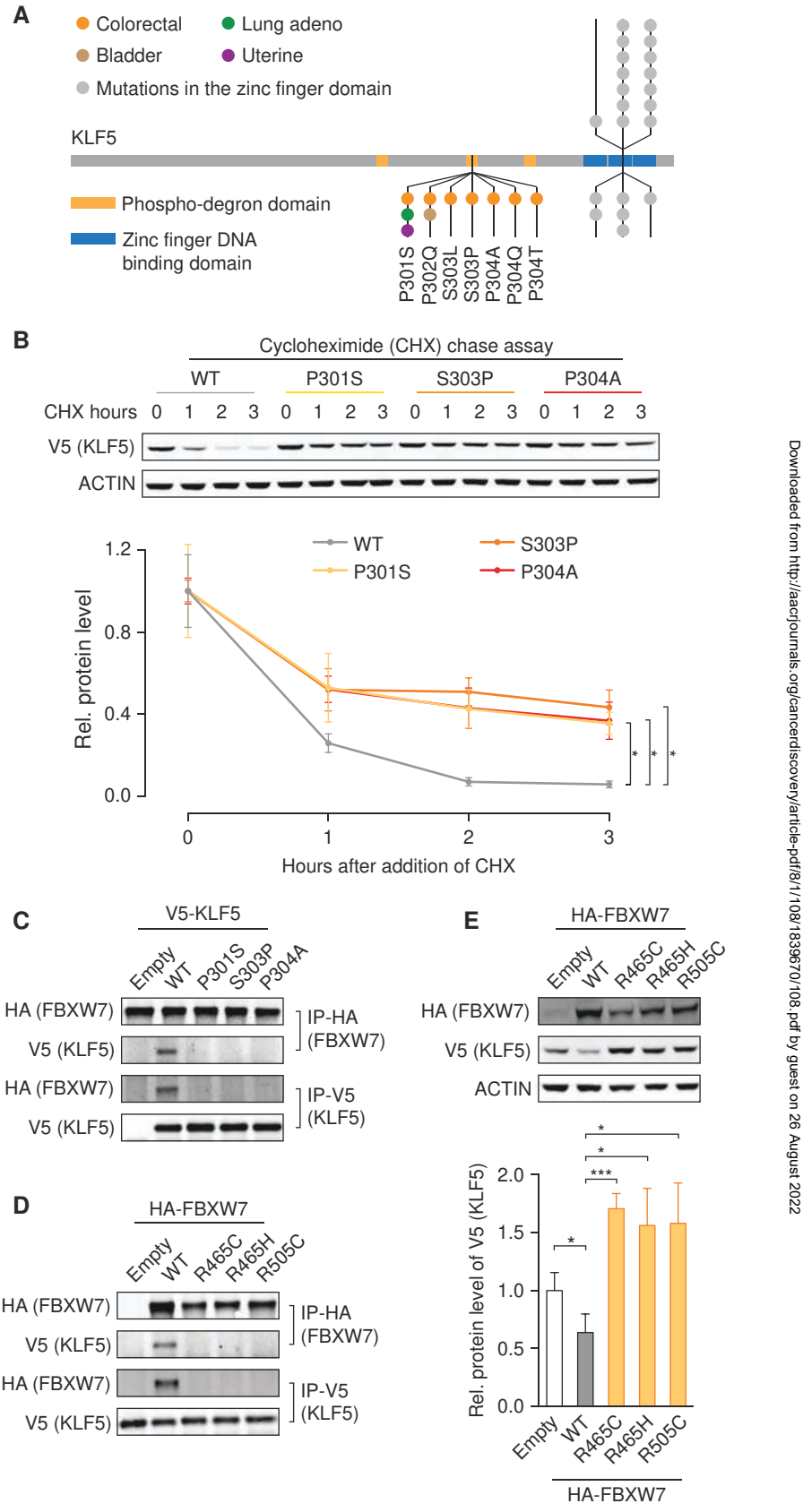

Figure 4. Functional characterization of *KLF5* hotspot mutations in a phospho-degron domain. **A,** Two mutation hotspots were identified in the *KLF5* gene in a phospho-degron domain, and in a ZNF DNA binding domain. Mutations in different cancer types are color coded. **B,** The colorectal cancer HCT116 cell line expressing V5-tagged WT KLF5, or KLF5 P301S, S303P, or P304A mutants, was treated with 100 ug/ml CHX for 0, 1, 2, and 3 hours, followed by immunoblotting for V5 and actin. Protein levels of WT and mutant KLF5 after CHX treatment was quantified ($n = 2$) and normalized to 0 hour (no treatment). Error bars, SD. *P* values were derived from student *t* tests: *, $P \le 0.05$. **C,** Coimmunoprecipitation assays using antibodies against V5 (tagged to KLF5) and HA (tagged to FBXW7) in HCT116 cells overexpressing V5-tagged KLF5 WT and mutants. **D,** Coimmunoprecipitation assays using antibodies against V5 (tagged to KLF5) and HA (tagged to FBXW7) in HCT116 cells overexpressing HA-tagged FBXW7 WT and mutants. **E,** Immunoblots show the protein level of V5-tagged KLF5 in HCT116 cells overexpressing HA-tagged FBXW7 WT and mutants. The protein level of V5-tagged KLF5 was quantified ($n = 3$) and normalized to HCT116 cells transfected with an empty vector. Error bars, SD. *P* values were derived from *t* tests: *, $P \le 0.05$; ***, $P \le 0.001$.

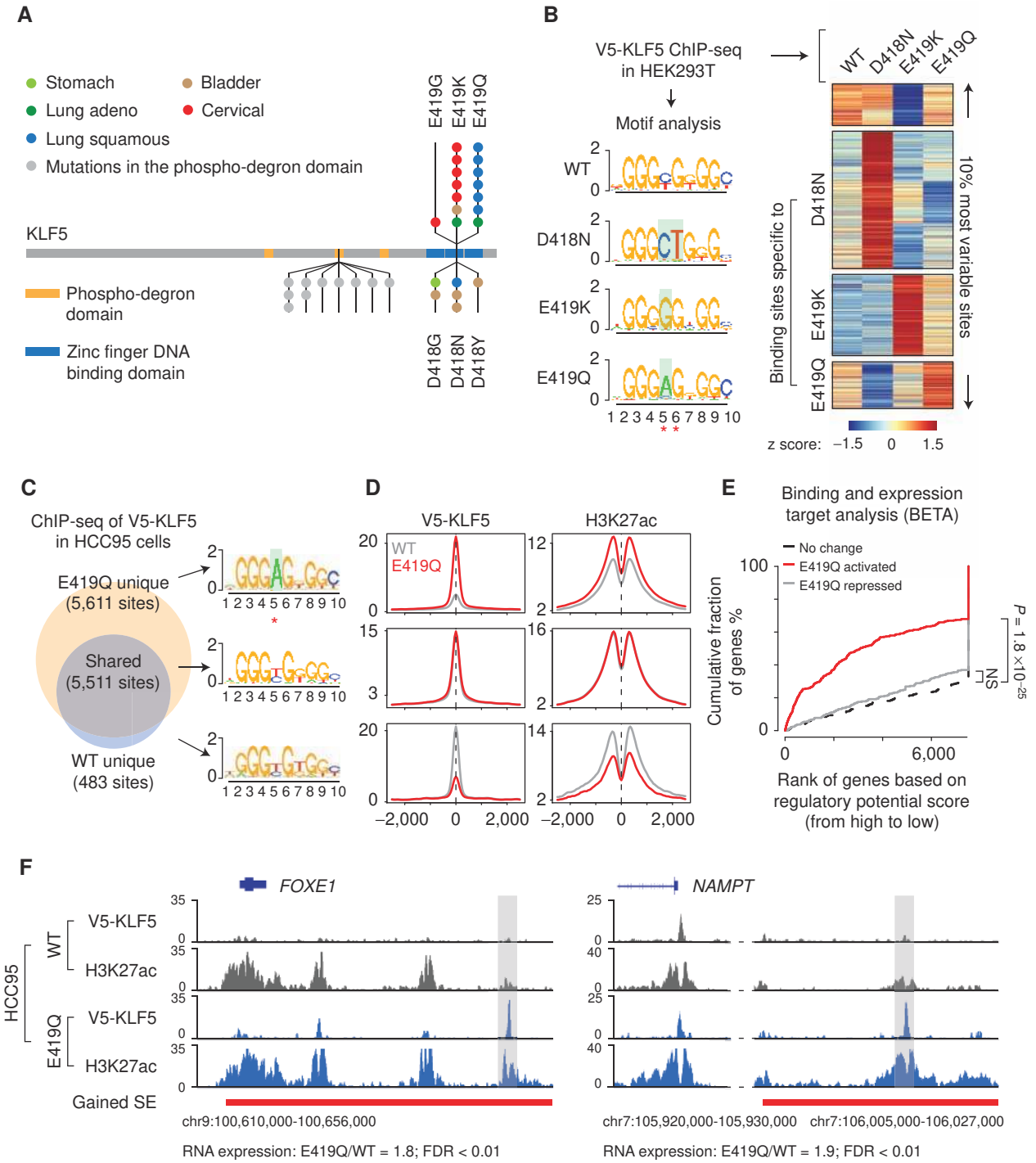

Figure 5. Functional characterization of *KLF5* hotspot mutations in a DNA binding domain. **A,** A *KLF5* mutation hotspot was identified in a ZNF DNA binding domain. Mutations in different cancer types are color coded. **B,** Left, ChIP-seq assays in HEK293T cells revealed the DNA binding motifs recognized by KLF5 WT and mutants. The nucleotide differences in the DNA binding motifs are highlighted by green boxes, and their positions are indicated by red asterisks. Right, the binding profile of KLF5 WT and mutants in the top 10% most variable KLF5 binding sites ($n = 1,165$). Normalization of the binding signal is described in the Methods section. **C,** Comparison of binding sites of KLF5 WT and E419Q in the lung squamous carcinoma cell line HCC95. DNA binding motifs are identified in the binding sites shared or unique to KLF5 WT and E419Q. **D,** Averaged ChIP-seq signal of V5-KLF5 (left) and H3K27ac (right), centered at the gained, shared, or lost binding sites of KLF5 E419Q, in HCC95 cells. **E,** BETA predicting the activating and repressive function of KLF5 E419Q. The 5,611 KLF5 E419Q–unique binding sites were used for the analysis. The gene expression data were derived from RNA-seq in the lung squamous carcinoma HCC95 cell line with KLF5 WT or E419Q overexpressed ($n = 2$). **F,** Examples of KLF5 E419Q target genes. ChIP-seq profile of V5 (KLF5) and H3K27ac in HCC95 cells overexpressing KLF5 WT or E419Q. The novel superenhancers associated with KLF5 E419Q are indicated. The fold change of the target genes *FOXE1* and *NAMPT* between HCC95 cells overexpressing KLF5 WT and E419Q, as measured by RNA-seq ($n = 2$), is indicated on the bottom.

To assess the function of these mutations, we generated N-terminal V5-tagged versions of WT KLF5 and three of the most recurrent mutants, D418N, E419K, and E419Q, and infected them into HEK293T cells (Supplementary Fig. S9A). ChIP-seq analysis of these cells revealed that the mutations in the DNA binding domain alter the DNA binding specificity of KLF5 in a mutation-specific manner (Fig. 5B). Changes in the cognate DNA binding motifs of KLF5 appeared to be predominantly restricted to nucleotides at the 5th and 6th positions of the DNA motifs (Fig. 5B), consistent with a report that the second ZNF domain of KLF transcription factors recognizes the 4–6th position of the DNA motif (76). The D418N mutant, seen in LUSC and BLCA, preferentially binds to thymidine (T) at the 6th nucleotide in the DNA motif, compared with guanine (G) for WT KLF5 (Fig. 5B). In addition, the E419K mutant, seen mainly in CESC, binds preferentially to G at the 5th nucleotide of the DNA motif, whereas the E419Q mutant, specific to lung cancers, binds preferentially to adenine (A) at the same nucleotide position, compared with cytosine (C) or T for WT KLF5 (Fig. 5B). Accordingly, KLF5 WT and mutant proteins bind to different regions of the genome (Fig. 5B). When KLF5 binding sites are ranked by variability among HEK293T cells overexpressing different WT or mutant constructs, ~44%, 26%, and 15% of the top 10% variable sites are preferentially bound by KLF5 D418N, E419K, and E419Q, respectively (Fig. 5B right panel for overview; Supplementary Fig. S9B for examples).

The KLF5 E419Q Mutant Gains Novel Binding Sites, Creates New Superenhancers, and Activates Cancer-Related Genes such as *FOXE1* and *NAMPT*

To study the function of mutations in the KLF5 DNA binding domain in a more physiologically relevant context, we analyzed the lung cancer–specific E419Q mutation in the lung squamous cancer cell line HCC95, which is WT for the *KLF5* gene based on RNA-seq results from the CCLE project (35). Ectopic expression and ChIP-seq analysis of V5-tagged KLF5 WT and KLF5 E419Q in HCC95 (Supplementary Fig. S10A-B) revealed that both WT and mutant KLF5 share 5,511 binding sites. Relative to KLF5 WT, however, KLF5 E419Q lost 483 binding sites and gained 5,611 new binding sites (Fig. 5C). Electrophoretic mobility shift assays (EMSA) using fluorescently labeled DNA probes containing the KLF5 DNA motifs with the C, T, and A variants at the 5th nucleotide revealed that KLF5 E419Q had a stronger binding affinity for the A variant, compared with WT KLF5 (Supplementary Fig. S10C), consistent with our results in HCC95 cells, above (Fig. 5C). However, like WT KLF5, KLF5 E419Q also binds to DNA motifs with the C and T variants (Supplementary Fig. S10C), which explains the observation that KLF5 E419Q gains more binding sites across the genome, compared with KLF5 WT. The regions that are specifically bound by KLF5 E419Q are more enriched in intronic regions (Fisher exact test: $P = 1.1 \times 10^{-42}$) and intergenic regions ($P = 1.3 \times 10^{-6}$) but less enriched in promoter regions ($P = 7.2 \times 10^{-86}$), compared with regions that are shared by KLF5 WT and KLF5 E419Q (Supplementary Fig. S10D), suggesting a shift from promoters to distal enhancers for the novel binding sites of KLF5 E419Q. We then investigated the effect of KLF5 E419Q binding on enhancer activity. In HCC95 cells overexpressing KLF5 E419Q, the gained binding sites show enrichment of H3K27ac, compared with cells overexpressing KLF5 WT (Fig. 5D).

We next performed gene expression analysis of HCC95 cells overexpressing untagged KLF5 WT or E419Q. Ectopic expression of either KLF5 WT or E419Q had little effect on the expression level of the endogenous *KLF5* gene, as measured by the PCR primers targeting the 3′UTR of *KLF5* (Supplementary Fig. S10B). By integrating the results of RNA-seq and ChIP-seq using the BETA pipeline, we found that the binding sites gained by KLF5 E419Q are significantly associated with activation of the target genes (Fig. 5E), suggesting a gene activation role for this mutant. Furthermore, the gained binding sites also form novel superenhancers, as defined by H3K27ac enrichment, that are associated with activation of genes such as *FOXE1, NAMPT, EPHB3,* and *GAS6* (Fig. 5F; Supplementary Fig. S10E). For instance, KLF5 E419Q binding occurring ~35 kb 3′ to the *FOXE1* gene leads to a marked increase in enhancer activity, as measured by the H3K27ac ChIP-seq profile, and the formation of a novel superenhancer that upregulates *FOXE1* expression as measured by RNA-seq (Fig. 5F). The *FOXE1* gene, encoding the Forkhead box protein E1, has been linked to thyroid cancer susceptibility (77), and inherited loss-of-function mutations of *FOXE1* cause cleft palate and hypothyroidism (78). Combined expression of *FOXE1* and *SOX2* has been shown to promote anchorage-independent growth of normal lung epithelial cell lines, suggesting an oncogenic role (1). Similarly, the binding of KLF5 E419Q ~95 kb upstream of *NAMPT* created a novel superenhancer and activated *NAMPT* expression (Fig. 5F). The *NAMPT* gene encodes nicotinamide phosphoribosyltransferase, a rate-limiting enzyme in the biosynthesis of the metabolite nicotinamide adenine dinucleotide (NAD; ref. 79). *NAMPT* is overexpressed in many cancer types, including colorectal, breast, gastric, and prostate cancers (80), and inhibition of NAMPT has been shown to impair tumor growth (81), suggesting its oncogenic function. In summary, our results indicate that the KLF5 E419Q mutant gains novel binding sites, creates new superenhancers, and activates genes implicated in tumorigenesis.

Cancer Cells with Activated *KLF5* Are Dependent on KLF5 for Their Proliferation

We next sought to investigate the phenotypic consequences of KLF5 activation in cancer cells. Silencing of *KLF5* using siRNAs in the HNSC cell line BICR31, in which *KLF5* overexpression is driven by the 13q22.1 superenhancer amplification (Fig. 2), resulted in a marked reduction of cell proliferation (Fig. 6A). In addition, multiplexed repression using KRAB–dCas9 and sgRNAs directed against the three enhancers e1, e3, and e4, that are amplified in head and neck squamous carcinomas (Fig. 2), also resulted in a significant reduction in proliferation of the BICR31 cell line (Fig. 6A). The proliferation-inhibitory effect of silencing *KLF5* can be partially rescued by ectopic expression of *ID1* (Fig. 6B), a target gene of KLF5 in head and neck squamous carcinoma cells (Fig. 3E and F). We then investigated the phenotypic outcomes of mutations in *KLF5*. Overexpression of the KLF5 E419Q mutant identified in lung squamous carcinomas

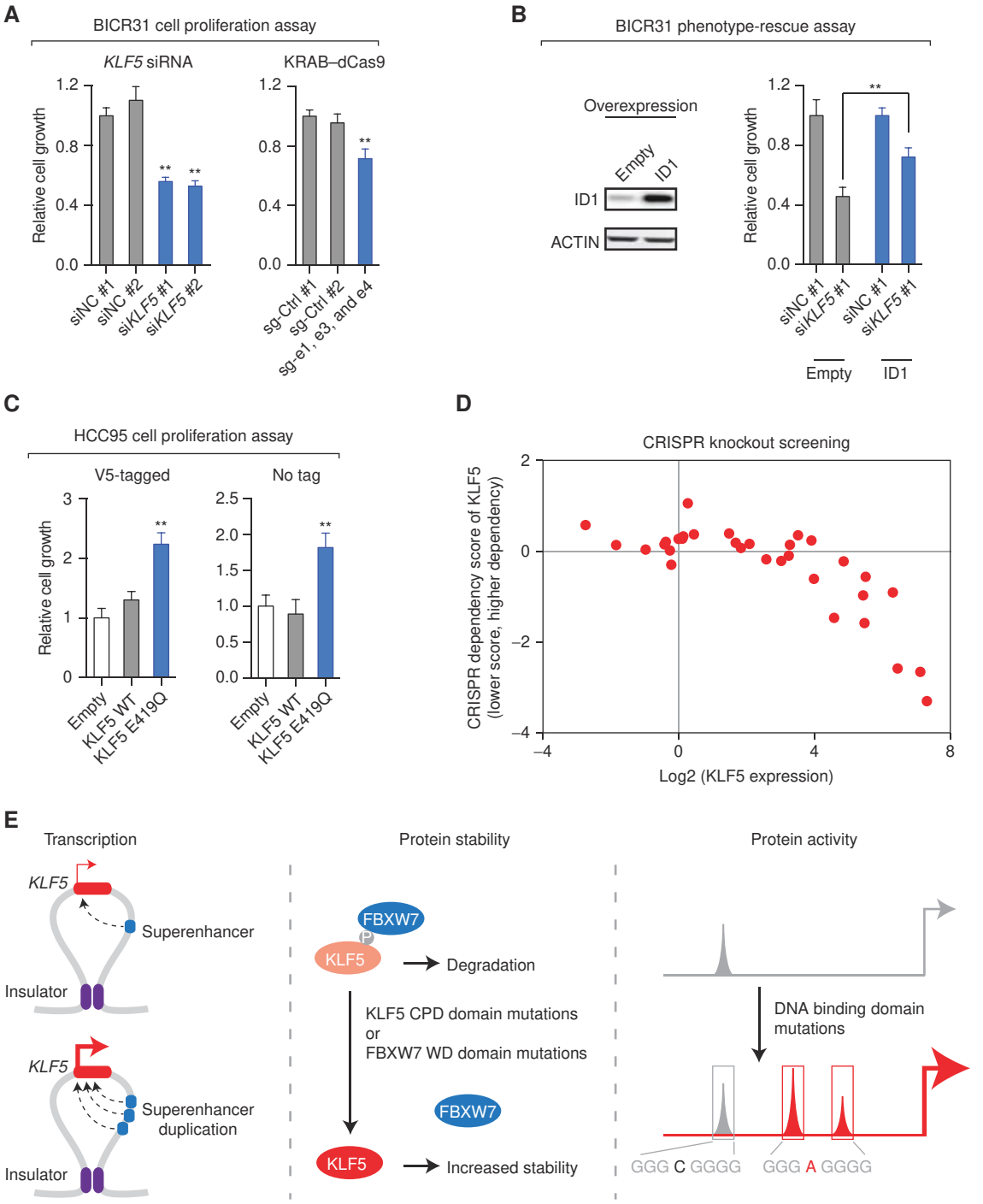

Figure 6. KLF5 activation confers a dependency of cancer cells on *KLF5*. **A,** Left, Cell proliferation assay of the head and neck squamous carcinoma cell line BICR31, with and without siRNA-mediated *KLF5* silencing ($n = 3$, cells were counted 6 days after transfection). Right, cell proliferation assay of BICR31 with and without KRAB–dCas9-mediated multiplexed repression of the e1, e3, and e4 enhancers of *KLF5* ($n = 3$, cells were counted 7 days after seeded). Cell number is normalized to the controls (siNC #1 or sg-Ctrl #1). Error bars, SD. *P* values were derived from *t* tests: **, $P \le 0.01$. **B,** Left, immunoblots showing the ectopic expression of ID1 protein in BICR31 cells. Right, overexpression of *ID1* rescued the proliferation-inhibitory effect of silencing *KLF5* in BICR31 cells ($n = 3$). Cell number is normalized to the controls (siNC #1-Empty or siNC #1-ID1). Error bars, SD. *P* values were derived from *t* tests: **, $P \le 0.01$. **C,** Cell proliferation assay in the lung squamous carcinoma cell line HCC95 overexpressing KLF5 WT or E419Q (with or without V5 tag), in low-serum (1% FBS) media ($n = 3$). Cell number is normalized to an empty vector control. Error bars, SD. *P* values were derived from *t* tests: **, $P \le 0.01$. **D,** The relationship between the gene expression level of *KLF5* (log2 transformed RNA-seq TPM, transcripts per million reads values) and CRISPR gene dependency ATARiS score (122) of *KLF5* across 32 cancer cell lines that were included in the Broad Institute GeCKO gene knockout screening (82). **E,** Schematic diagram: KLF5 can be activated on the transcriptional level by noncoding superenhancer amplifications, on the protein level by missense mutations in a CPD phospho-degron domain of KLF5 or in the WD40-repeat protein interaction domains of FBXW7, and on the activity level by missense mutations in a ZNF DNA binding domain of KLF5.

significantly increased proliferation of the LUSC cell line HCC95, compared with KLF5 WT, in low-serum media (Fig. 6C), suggesting an oncogenic role for the KLF5 E419Q mutant.

We next asked whether activation of KLF5 correlates with a dependency of cancer cells on the *KLF5* gene. We queried the publicly available genome-wide CRISPR/Cas9 gene knockout screening (GeCKO) dataset, including 32 cancer cell lines originating from diverse tissue types such as bone, skin, colon, and pancreas (82). Gene dependency scores were calculated based on the abundance of each sgRNA before and after cell proliferation for 3–4 weeks following infection of the library; gene expression was measured by RNA-seq (82). We found that cancer cells with higher *KLF5* expression were more dependent on *KLF5* (i.e., exhibited a lower gene dependency score), suggesting that increased expression of *KLF5* confers a dependency on the *KLF5* gene for cell viability (Fig. 6D). Because none of the 32 cell lines used in this analysis bear *KLF5* coding mutations, we could not investigate the dependency of KLF5 mutants.

DISCUSSION

Here, we describe the functional analysis of the altered *KLF5* gene, with findings that support the concept of an oncogenic role for *KLF5*. These discoveries are based on the identification of somatic cancer genome alterations in or near the *KLF5* gene (15, 22). Our pan-cancer analysis showed that *KLF5* is activated by multiple somatic genomic alterations, including noncoding superenhancer amplifications and coding mutations in a phospho-degron domain or a DNA binding domain (Fig. 6E). The frequency of individual types of *KLF5* genomic alterations is modest. However, the combination of the three types of alterations markedly enhances the significance of *KLF5* as a candidate oncogene. This work extends and provides a mechanistic basis for previous observations that overexpression of WT *KLF5* promotes oncogenic phenotypes such as cellular proliferation, invasion, and transformation *in vitro* and *in vivo* (27–31).

We have identified focal amplifications of *KLF5* noncoding superenhancers in many squamous cell carcinomas and some adenocarcinomas. In contrast to the *MYC* locus, in which cancer type–specific superenhancers are amplified (15), the same noncoding region ~300 kb 3′ to *KLF5* is amplified in multiple anatomic and histologic forms of cancer. This may occur because, in contrast to the *MYC* locus, the enhancer profile of the *KLF5* locus is shared across different cancer types. We and others have identified single individual enhancers within superenhancers that drive the activity of the entire superenhancer region (15, 83). In contrast, the activity of the *KLF5* superenhancer region is dependent on a combination of three individual enhancers, representing another type of enhancer structure within superenhancers.

In addition to transcriptional regulation, we show that KLF5 is activated at the protein level by missense mutations. KLF5 contains three CPD domains, which, upon phosphorylation, are recognized by the E3 ubiquitin ligase FBXW7 that promotes ubiquitination and degradation of its substrates (70). Studies have shown that several oncogenic proteins, including CCNE1, MYC, and NOTCH1, are substrates of FBXW7 (84–86) and are stabilized by mutations in the FBXW7 WD40 repeat domains required for substrate recognition (74, 75, 87). Our studies show that KLF5 is a substrate of FBXW7 in colorectal cancers, and that mutations either in a phospho-degron domain of KLF5 or in the WD40-repeat domains of FBXW7 stabilize KLF5 protein levels by preventing the interaction of KLF5 and FBXW7. The observation that no colorectal cancer samples have both *KLF5* CPD mutations and coding *FBXW7* mutations further supports their functional convergence. This mirrors the mutation pattern of the E3 ligase gene *KEAP1* and the oncogenic transcription factor gene *NFE2L2*, which encodes a substrate of KEAP1, in lung cancer (16, 88). We expect that detailed characterization of protein domain interactions combined with mutual exclusivity analysis of genomic alterations will identify more such relationships between cancer-related genes.

Another mutation hotspot in the *KLF5* gene was identified in a ZNF DNA binding domain. We find that these mutations promote a change-of-function role, by altering KLF5 DNA binding specificity. Our observations are consistent with recent findings reporting recurrent mutations in *KLF4,* another KLF family member gene, in meningiomas (89). Unlike *KLF5* that is mutated in the second ZNF domain that recognizes the 4–6th nucleotide position of the KLF DNA motif, *KLF4* is mutated in the first ZNF domain that binds to the 7–10th nucleotides (76, 89). Accordingly, the DNA motifs recognized by KLF5 and KLF4 mutants are different from the canonical KLF motif at the 5–6th and 9th nucleotide position, respectively (89). This suggests distinct oncogenic roles for these two KLF family members in their respective cancer types. Interestingly, although *KLF5* change-of-function mutations occur within a single ZNF domain, each mutation is highly cancer type–specific. Moreover, different mutations guide KLF5 to recognize different DNA sequences, suggesting that individual KLF5 mutants direct unique gene expression programs to drive tumorigenesis via distinct mechanisms in the relevant tumor types.

We showed that the lung cancer–specific KLF5 E419Q mutant gains novel binding sites in the genome relative to WT KLF5 while also maintaining the binding sites of the WT protein. This result contrasts with the finding of change-of-function mutations in *TP53* that lead to a switch in the DNA binding specificity of p53 toward novel binding sites while eliminating binding sites recognized by WT p53 (90, 91). This difference may be because, unlike the tumor suppressor p53, WT KLF5 itself is an oncogenic transcription factor and thus losing WT KLF5 binding sites may be disadvantageous to cancer cells. The gained binding sites of KLF5 E419Q are associated with gene activation, as evident by the increased enhancer activity at these binding sites. Importantly, the newly acquired KLF5 E419Q binding sites also create novel superenhancers that drive expression of cancer-associated genes such as *FOXE1* and *NAMPT*, revealing new therapeutic targets. In addition to *KLF5*, somatic hotspot mutations have been identified in the DNA binding domains of other transcription factors such as FOXA1 and MAX (92, 93). Furthermore, many germline genetic variants in genes encoding transcription factors have been predicted to alter DNA binding activity and specificity (94). Future studies focused on deeper

functional characterization of these somatic and germline variants will likely uncover the specific mechanisms underlying their pathogenic features.

In addition to somatic genetic alterations, noncoding germline genetic variants near the *KLF5* gene have been associated with the development of prostate, pancreatic, and endometrial cancers (95–100). This is reminiscent of the noncoding region near the *MYC* oncogene, where genetic variants have been associated with predisposition to multiple cancers (101). It is known that cancer risk–associated variants often target regulatory elements, modulate transcription factor binding, and regulate expression of cancer-related genes (102–106). Interestingly, some of the cancer-risk variants near *KLF5*, such as rs9573163 and rs9543325, that are associated with pancreatic cancer risk (97, 99, 100), are within the superenhancer regions that we found to be amplified in squamous carcinomas. The functional relevance of the 13q22.1 genetic-risk variants in regulating *KLF5* and cancer development needs further investigation.

In summary, we demonstrate that a single oncogenic transcription factor, KLF5, can be activated by multiple somatic genomic alterations including by the creation of noncoding structural genome variations and by hotspot missense mutations within the *KLF5* coding region. Importantly, we show that overexpression of KLF5 is associated with a strong dependency on KLF5 across 32 cancer cell lines. In addition, targeting KLF5 *in vivo* has been reported as an efficient antitumor strategy for breast, bladder, and gastric cancers (28, 30, 107, 108). All the evidence indicates the importance of KLF5 activation in cancer cells and its significance as an emerging target for the development of cancer therapeutics.

METHODS

Pan-Cancer Copy-Number Alteration Analysis

Genomic identification of significant targets in cancer (GISTIC) analyses were performed in 10,844 samples from 33 tumor types, using copy-number data from version 3.0 of the SNP pipeline on April 2, 2015, from the TCGA copy-number portal (2, 109). Arm-level amplifications or deletions were removed for GISTIC peak calling.

Cell Lines

Cell lines were obtained from the CCLE project (35) in 2015 and 2016. Cells tested negative for *Mycoplasma* and were maintained in RPMI-1640 medium supplemented with 10% heat-inactivated FBS and 1% penicillin streptomycin. Cell line identities were verified by SNP fingerprinting using an Affymetrix SNP array as previously described in the CCLE project (35). Cell lines were used for functional experiments, after less than 3 months of passages post receipt.

ChIP-seq Analysis

ChIP-seq assays were performed as previously described (102, 105). Briefly, cells were cross-linked with 1% formaldehyde and lysed. The chromatin extract was sonicated by a Diagenode bioruptor and immunoprecipitated with antibodies that were coincubated with mixed Dynabeads A and G (Thermo Scientific). Antibodies that were used include H3K27ac (2 μg per ChIP; Abcam, ab4729), KLF5 (4 μg per ChIP; Abcam, ab137676), p300 (4 μg per ChIP; Bethyl Lab, A300-358), and V5 (4 μg per ChIP; Thermo Fisher, R960-25). The sequencing libraries were prepared using the NEB ChIP-seq library prep kit (NEB, E6200L) and sequenced on the Illumina MiSeq instrument (50-bp single read reads). Sequencing reads were aligned to the hg19 human genome reference by the Burrows–Wheeler Aligner (BWA; refs. 110, 111), and ChIP-seq binding sites were identified by MACS2 (111). Motif search was performed by using the SeqPos motif tool in the Cistrome pipeline (59).

For investigating the effect of KLF5 silencing on the H3K27ac profile (Supplementary Fig. S6), we used the "DNaseI Hypersensitive Site Master List" file generated by the ENCODE consortium (112) to identify open chromatin regions that are conserved across cell types and used them as "negative controls." We selected the regions that are enriched with DNase I-hypersensitivity signal in more than half of the 125 ENCODE cell types included in the list and removed the ones that overlap with KLF5 bindings.

For clustering binding sites of KLF5 WT and mutants in HEK293T cells, we first concatenated and merged all of their binding sites identified by MACS2 and then mapped the sequencing reads to each of the merged binding sites by Bedtools (113). The number of reads at these binding sites was normalized by edgeR pipeline (114, 115) and then $\log_2$ transformed. We performed k-means clustering for the top 10% most variable binding sites. To present the heat map, the normalized binding signal was scaled by rows. For identifying binding sites that are specific to KLF5 WT or E419Q in the LUSC cell line HCC95, we used MACS2 and compared the ChIP-seq signal of V5-tagged KLF5 WT and E419Q by using each other as "treatment" and "control" for MACS2 input. For comparing the H3K27ac ChIP-seq signal between KLF5 E419Q and WT binding sites, because the difference of total sequencing reads between the ChIP-seq experiments is over 10%, we randomly subsampled the larger sample by Samtools (116) to normalize the signal. ChIP-seq data were uploaded to the Gene Expression Omnibus (GEO; GSE88976).

Superenhancer Identification

For each cancer type, H3K27ac ChIP-seq data from multiple cell lines were merged into one dataset. Based on the merged ChIP-seq results, including the aligned reads and MACS2 binding peaks, we identified superenhancers for each cancer type using the ROSE pipeline (39–41). To identify superenhancers that are gained by KLF5 E419Q bindings, we used Bedtools (113) to compare the superenhancers called from H3K27ac ChIP-seq signal in HCC95 cells overexpressing KLF5 WT and E419Q. We identified the superenhancers that have >75% region unique to cells overexpressing KLF5 E419Q and also overlap with KLF5 E419Q–specific binding sites. Genomic coordinates of the KLF5 E419Q–gained superenhancers and the nearest genes are listed in Supplementary Table S1.

3C Assay

3C-qPCR assays were performed in BICR31 and BICR6 cells, as previously described (42, 105). The restriction enzyme BglII was used to fragment DNA. BAC libraries (RP11-689G3, RP11-179I20, RP11-259I24, RP11-343F2, RP11-315L12, RP11-347N11, and RP11-46L3) of DNA fragments covering the tested regions were used as template controls for the normalization of digestion, ligation, and primer efficiency. In order to normalize the DNA copy number in BICR31 cells, we doubled the input concentration of the BAC construct RP11-343F2 that covers the superenhancer region. The 3C ligation products were quantified by SYBR Green-based PCR and the primer sequences are listed in Supplementary Table S2.

CRISPR/Cas9-Mediated Enhancer Repression

CRISPR/Cas9 sgRNAs were identified using the sgRNA designer tool from the Broad Institute (117) and control, nontargeting sgRNAs were selected from the GeCKOv2 library (118). The enhancer repression vector lenti-KRAB–dCas9-blast was generated previously

(15) and sgRNAs were cloned into lentiGuide-Puro (Addgene, 52963). BICR31 cells were first infected with lenti-KRAB–dCas9-blast and selected with 6 μg/mL blasticidin, and then subsequently infected with lentiGuide-sgRNAs and selected with 2 μg/mL puromycin. For multiplexed repression of the e1, e3, and e4 enhancers, lentivirus containing each sgRNA was mixed equally and then used for cell infection. sgRNA sequences were listed in Supplementary Table S2.

Luciferase Reporter Assays

Luciferase reporter assays were performed as previously described (15). Individual enhancer regions were cloned upstream of the pGL3 minimal promoter vector using MluI and XhoI restriction enzyme sites. For cloning the three enhancers e1, e3, and e4 together into the vector, we used the Gibson assembly cloning method (NEB E2611S) that ligated multiple fragments by their overlaps. The reporter constructs were cotransfected with a control *Renilla* luciferase construct into cells using FuGENE 6 (Promega). The luciferase signal was normalized to the *Renilla* luciferase signal. Primers used for cloning are listed in Supplementary Table S2.

siRNA-Directed Gene Silencing

BICR31 cells were transfected with negative control, nontargeting siRNA (siNC), or si*KLF5* using Lipofectamine RNAiMAX (Thermo Scientific). RNA was extracted 2 days after transfection using the Qiagen RNeasy kit with on-column DNase I treatment. Preverified Silencer Select siRNAs (Thermo Scientific, Negative Control Nos.1 and 2 for siNC; s2115 and s2116 for si*KLF5*) were used. siNC #1 and si*KLF5* #1 were used for RNA-seq assays with three biological replicates in BICR31 cells, and all the siRNAs were used for gene expression validation. To assess the effect of siRNAs, immunoblot analysis was performed using antibodies against KLF5 (Abcam, ab137676) and β-actin (Santa Cruz, sc-47778).

Identification of KLF5 *Mutation Hotspots*

To estimate the significance of mutation frequency within hotspots in the *KLF5* gene, we computed *P* values for a sliding fixed-width window over the primary structure of *KLF5*. We implemented a binomial null distribution with n as the total number of *KLF5* mutations and p as the fraction of the primary structure of KLF5 represented by our window. The *P* value was then computed as the survival function of the binomial distribution where k+1 is the number of mutations actually present in the window. Windows of 3 amino acids and 5 amino acids were used to analyze the TCGA Pan-Cancer data set (64) and the colorectal cancer data set (23), respectively.

Ectopic Expression of KLF5 and FBXW7

WT *KLF5* and *FBXW7* cDNA were first cloned into pJET1.2 (Thermo Scientific). Quik-change mutagenesis was then performed to generate cDNA of *KLF5* mutants (P301S, S303P, P304A, D418N, E419K, and E419Q) and *FBXW7* mutants (R465C, R465H, and R505C). The *KLF5* and *FBXW7* (WT and mutants) cDNA were then subcloned into the overexpression vector pLenti-EF1a-PGK-puro and pLenti-EF1a-PGK-blasti, respectively, with or without the V5 tag fused to the N-terminus. Infected HEK293T and HCC95 cells were selected by 2 μg/mL puromycin or 10 μg/mL blasticidin. Overexpression was validated by RT-PCR and immunoblot analysis. Primers used for cloning are listed in Supplementary Table S2.

Cell Proliferation Assays

For si*KLF5* experiments, BICR31 cells were transfected with siNC1 (#1 and #2) or si*KLF5* (#1 and #2) and were then maintained in regular media for 6 days before cell counting (Beckman Coulter Counter). For CRISPR-mediated enhancer repression experiments, BICR31 cells infected with sg-Control (#1 and #2), or combined sg-e1, e3, and e4 were selected by 2 μg/mL puromycin for 5 days. Cells were then seeded at the same cell number and maintained in regular media for 7 days before cell counting. For KLF5 WT versus E419Q overexpression experiments, HCC95 cells infected with KLF5 WT and E419Q overexpression constructs (with or without V5 tagged) were maintained in low-serum condition (RPMI-1640 media supplemented with 1% FBS) for 7 days before cell counting.

RNA-seq Analysis

For si*KLF5* experiments, BICR31 cells transfected with siNC #1 and si*KLF5* #1 (three biological replicates each condition) were maintained in regular media for 2 days before RNA extraction. For KLF5 WT versus E419Q overexpression experiments, HCC95 cells infected with KLF5 WT and E419Q overexpression constructs (no-tagged, two biological replicates) were maintained in low-serum condition (RPMI-1640 media supplemented with 1% FBS), which is consistent with the condition of cell proliferation assays of KLF5 E419Q overexpression, for 2 days before RNA extraction. RNA was extracted using Qiagen RNeasy kit and treated with on-column DNase I. RNA-seq libraries were prepared using the NEBNext Ultra Directional RNA library prep kit (NEB, E7420S) and sequenced on the Illumina MiSeq instrument (75-bp paired end reads). Sequencing reads were aligned using STAR (119), and expression level for each gene was quantified by RSEM (120). The differential expression analysis was performed using the edgeR and limma pipelines (115, 121). The RNA-seq results were uploaded to the GEO (GSE88977).

BETA Analysis to Combine ChIP-seq and RNA-seq Results

BETA was performed to predict whether KLF5 has activating or repressive function by combining ChIP-seq and RNA-seq results. The analysis pipeline was described as previously described (63). Briefly, BETA estimates KLF5's regulatory potential score for each gene based on the distance between KLF5 binding sites and TSSs of each gene, and also based on the number of KLF5 binding sites ±50 kb centered at TSS of each gene. BETA then uses a nonparametric statistical test (Kolmogorov–Smirnov test) to compare regulatory potential scores for genes that are upregulated, downregulated, or not regulated on the basis of RNA-seq results with and without siRNA-mediated silencing of *KLF5*. Similarly, we performed BETA analysis for analyzing KLF5 E419Q–unique binding sites and genes that are regulated by KLF5 E419Q overexpression (compared with KLF5 WT) in HCC95 cells.

Quantitative PCR

Quantitative PCR (qPCR) was performed using TaqMan Universial PCR Mastermix or Power SYBR green PCR Mastermix (Thermo Fisher) on a Bio-Rad C1000-Touch Real-time PCR instrument. For TaqMan PCR, the following premade 5′ nuclease probes were ordered from Integrated DNA technologies: KLF5 (Hs.PT.56a.40282397), KLF12 (Hs.PT.58.28103949), PIBF1 (Hs.PT.58.21509866), DIS3 (Hs.PT.58.39902044), ID1 (Hs.PT.58.18791272.g), and internal references HPRT1 (Hs.PT.58v.45621572; for qPCR signal normalization) and GAPDH (Hs.PT.58.589810.g). For SYPR green PCR, the primers used are listed in Supplementary Table S2.

CHX Chase Assays

HEK293T cells infected with *KLF5* WT, P301S, S303P, or P304A were treated with 100 μg/mL CHX for 0, 1, 2, and 3 hours before protein extraction and immunoblot analysis. The protein level of KLF5 WT and mutants was quantified by using the LI-COR Image Studio software.

Coimmunoprecipitation Assays

Antibodies were first incubated with mixed Dynabeads A and G (Thermo Fisher) for 5 hours at 4°C. Cells were lysed by cell lysis

buffer (1% NP40, 150 mmol/L NaCl, 50 mmol/L Tris-HCl pH 8.0) supplemented with protease and phosphotase inhibitor. Antibodies that were used include V5 (4 μg per IP; Thermo Fisher, R960-25) and HA (4 μg per IP; Abcam, ab9110). Cell lysate were then incubated with the beads–antibody complex. Enriched protein was eluted and denatured at 65°C by LDS sample buffer (Thermo Fisher) supplemented with 20 mmol/L DTT before immunoblot analysis.

EMSA Assays

KLF5 WT and E419Q proteins were translated by using the TNT Quick Coupled Transcription/Translation System (Promega L1170). The translated protein was verified by immunoblot analysis using the KLF5 antibody (Abcam, ab137676). The fluorescent DNA probes containing KLF5 motifs were made from Integrated DNA Technologies and their sequences were listed in Supplementary Table S2. For the EMSA, the translated KLF5 proteins and the DNA probes were mixed, and incubated with binding reaction buffer (Final concentration: 10 mmol/L Tris-HCL pH 7.5, 50 mmol/L KCl, 2.5 mmol/L DTT, 0.05 mmol/L EDTA, 0.05 μg/μL Poly-dIdC, 0.25% Tween20) for 30 minutes at room temperature. The reaction mix was added with orange loading dye and loaded on a Tris/Borate/EDTA (TBE) gel. Images were taken on a LI-COR instrument.

Accession Codes

The newly generated ChIP-seq and RNA-seq data have been deposited to the GEO public dataset under the series GSE88976 and GSE88977, respectively.

Disclosure of Potential Conflicts of Interest

J.M. Francis is a senior scientist at Gritstone Oncology and has ownership interest (including patents) in the same. G.F. Gao reports receiving commercial research support from Bayer AG. A.C. Berger reports receiving commercial research support from Bayer AG. A.D. Cherniack reports receiving a commercial research grant from Bayer AG. M. Meyerson reports receiving a commercial research grant from Bayer, has ownership interest in Origimed, and is a consultant/advisory board member for Origimed. No potential conflicts of interest were disclosed by the other authors.

Authors' Contributions

Conception and design: X. Zhang, M. Meyerson
Development of methodology: X. Zhang, W.C. Hahn, A.D. Cherniack
Acquisition of data (provided animals, acquired and managed patients, provided facilities, etc.): X. Zhang, F. Vazquez, J. Zhou, Z. Wu, M. Giannakis, W.C. Hahn
Analysis and interpretation of data (e.g., statistical analysis, biostatistics, computational analysis): X. Zhang, J.M. Francis, G.F. Gao, J.D. Campbell, Y. Mitsuishi, G. Ha, J. Shih, F. Vazquez, A. Tsherniak, A.M. Taylor, A.C. Berger, M. Giannakis, A.D. Cherniack
Writing, review, and/or revision of the manuscript: X. Zhang, P.S. Choi, J.M. Francis, G.F. Gao, J.D. Campbell, A. Ramachandran, Y. Mitsuishi, A. Tsherniak, M. Giannakis, W.C. Hahn, M. Meyerson
Administrative, technical, or material support (i.e., reporting or organizing data, constructing databases): X. Zhang, P.S. Choi
Study supervision: W.C. Hahn, M. Meyerson

Acknowledgments

We thank members of the Meyerson laboratory for discussions. We thank Craig Strathdee, Hugh Gannon, and Lior Golomb for reagents.

Grant Support

We acknowledge support from the National Cancer Institute to M. Meyerson (1R35CA197568), National Cancer Institute Pathway to Independence awards to X. Zhang (1K99CA215244) and P.S. Choi (1K99CA208028), and the Norman R. Seaman Endowment fund to M. Meyerson. M. Meyerson is an American Cancer Society Research Professor.

Received May 17, 2017; revised September 18, 2017; accepted September 26, 2017; published OnlineFirst September 29, 2017.

REFERENCES

1. Bass AJ, Watanabe H, Mermel CH, Yu S, Perner S, Verhaak RG, et al. SOX2 is an amplified lineage-survival oncogene in lung and esophageal squamous cell carcinomas. Nat Genet 2009;41:1238–42.
2. Beroukhim R, Mermel CH, Porter D, Wei G, Raychaudhuri S, Donovan J, et al. The landscape of somatic copy-number alteration across human cancers. Nature 2010;463:899–905.
3. Garraway LA, Widlund HR, Rubin MA, Getz G, Berger AJ, Ramaswamy S, et al. Integrative genomic analyses identify MITF as a lineage survival oncogene amplified in malignant melanoma. Nature 2005;436:117–22.
4. Visakorpi T, Hyytinen E, Koivisto P, Tanner M, Keinänen R, Palmberg C, et al. In vivo amplification of the androgen receptor gene and progression of human prostate cancer. Nat Genet 1995;9:401–6.
5. Little CD, Nau MM, Carney DN, Gazdar AF, Minna JD. Amplification and expression of the c-myc oncogene in human lung cancer cell lines. Nature 1983;306:194–6.
6. Schwab M, Alitalo K, Klempnauer K-H, Varmus HE, Bishop JM, Gilbert F, et al. Amplified DNA with limited homology to myc cellular oncogene is shared by human neuroblastoma cell lines and a neuroblastoma tumour. Nature 1983;305:245–8.
7. Bandopadhayay P, Ramkissoon LA, Jain P, Bergthold G, Wala J, Zeid R, et al. MYB-QKI rearrangements in angiocentric glioma drive tumorigenicity through a tripartite mechanism. Nat Genet 2016;48:273–82.
8. Battey J, Moulding C, Taub R, Murphy W, Stewart T, Potter H, et al. The human c-myc oncogene: structural consequences of translocation into the IgH locus in Burkitt lymphoma. Cell 1983;34:779–87.
9. Beroukhim R, Zhang X, Meyerson M. Copy number alterations unmasked as enhancer hijackers. Nat Genet 2016;49:5–6.
10. Drier Y, Cotton MJ, Williamson KE, Gillespie SM, Ryan RJH, Kluk MJ, et al. An oncogenic MYB feedback loop drives alternate cell fates in adenoid cystic carcinoma. Nat Genet 2016;48:265–72.
11. Tomlins SA, Rhodes DR, Perner S, Dhanasekaran SM, Mehra R, Sun X-W, et al. Recurrent fusion of TMPRSS2 and ETS transcription factor genes in prostate cancer. Science 2005;310:644–8.
12. Kron KJ, Murison A, Zhou S, Huang V, Yamaguchi TN, Shiah Y-J, et al. TMPRSS2-ERG fusion co-opts master transcription factors and activates NOTCH signaling in primary prostate cancer. Nat Genet 2017;49:1336–45.
13. Herranz D, Ambesi-Impiombato A, Palomero T, Schnell SA, Belver L, Wendorff AA, et al. A NOTCH1-driven MYC enhancer promotes T cell development, transformation and acute lymphoblastic leukemia. Nat Med 2014;20:1130–7.
14. Shi J, Whyte WA, Zepeda-Mendoza CJ, Milazzo JP, Shen C, Roe J-S, et al. Role of SWI/SNF in acute leukemia maintenance and enhancer-mediated Myc regulation. Genes Dev 2013;27:2648–62.
15. Zhang X, Choi PS, Francis JM, Imielinski M, Watanabe H, Cherniack AD, et al. Identification of focally amplified lineage-specific super-enhancers in human epithelial cancers. Nat Genet 2016;48:176–82.
16. The Cancer Genome Atlas Research Network. Comprehensive genomic characterization of squamous cell lung cancers. Nature 2012;489:519–25.
17. Shibata T, Ohta T, Tong KI, Kokubu A, Odogawa R, Tsuta K, et al. Cancer related mutations in NRF2 impair its recognition by Keap1-Cul3 E3 ligase and promote malignancy. Proc Natl Acad Sci 2008;105:13568–73.

18. Bailey SD, Desai K, Kron KJ, Mazrooei P, Sinnott-Armstrong NA, Treloar AE, et al. Noncoding somatic and inherited single-nucleotide variants converge to promote ESR1 expression in breast cancer. Nat Genet 2016;48:1260–6.
19. Mansour MR, Abraham BJ, Anders L, Berezovskaya A, Gutierrez A, Durbin AD, et al. Oncogene regulation. An oncogenic super-enhancer formed through somatic mutation of a noncoding intergenic element. Science 2014;346:1373–7.
20. Deng N, Goh LK, Wang H, Das K, Tao J, Tan IB, et al. A comprehensive survey of genomic alterations in gastric cancer reveals systematic patterns of molecular exclusivity and co-occurrence among distinct therapeutic targets. Gut 2012;61:673–84.
21. Giefing M, Wierzbicka M, Rydzanicz M, Cegla R, Kujawski M, Szyfter K. Chromosomal gains and losses indicate oncogene and tumor suppressor gene candidates in salivary gland tumors. Neoplasma 2008;55:55–60.
22. Campbell JD, Alexandrov A, Kim J, Wala J, Berger AH, Pedamallu CS, et al. Distinct patterns of somatic genome alterations in lung adenocarcinomas and squamous cell carcinomas. Nat Genet 2016;48:607–16.
23. Giannakis M, Mu XJ, Shukla SA, Qian ZR, Cohen O, Nishihara R, et al. Genomic correlates of immune-cell infiltrates in colorectal carcinoma. Cell Rep 2016;15:857–65.
24. Takahashi K, Yamanaka S. Induction of pluripotent stem cells from mouse embryonic and adult fibroblast cultures by defined factors. Cell 2006;126:663–76.
25. Shields JM, Christy RJ, Yang VW. Identification and characterization of a gene encoding a gut-enriched Krüppel-like factor expressed during growth arrest. J Biol Chem 1996;271:20009–17.
26. Sun R, Chen X, Yang VW. Intestinal-enriched Krüppel-like factor (Krüppel-like factor 5) is a positive regulator of cellular proliferation. J Biol Chem 2001;276:6897–900.
27. Jia L, Zhou Z, Liang H, Wu J, Shi P, Li F, et al. KLF5 promotes breast cancer proliferation, migration and invasion in part by upregulating the transcription of TNFAIP2. Oncogene 2016;35:2040–51.
28. Qin J, Zhou Z, Chen W, Wang C, Zhang H, Ge G, et al. BAP1 promotes breast cancer cell proliferation and metastasis by deubiquitinating KLF5. Nat Commun 2015;6:8471.
29. Chen C, Benjamin MS, Sun X, Otto KB, Guo P, Dong X-Y, et al. KLF5 promotes cell proliferation and tumorigenesis through gene regulation and the TSU-Pr1 human bladder cancer cell line. Int J Cancer 2006;118:1346–55.
30. Chia N-Y, Deng N, Das K, Huang D, Hu L, Zhu Y, et al. Regulatory crosstalk between lineage-survival oncogenes KLF5, GATA4 and GATA6 cooperatively promotes gastric cancer development. Gut 2015;64:707–19.
31. Nandan MO, McConnell BB, Ghaleb AM, Bialkowska AB, Sheng H, Shao J, et al. Krüppel-like factor 5 mediates cellular transformation during oncogenic KRAS-induced intestinal tumorigenesis. Gastroenterology 2008;134:120–30.
32. Nakaya T, Ogawa S, Manabe I, Tanaka M, Sanada M, Sato T, et al. KLF5 regulates the integrity and oncogenicity of intestinal stem cells. Cancer Res 2014;74:2882–91.
33. Fujii Y, Yoshihashi K, Suzuki H, Tsutsumi S, Mutoh H, Maeda S, et al. CDX1 confers intestinal phenotype on gastric epithelial cells via induction of stemness-associated reprogramming factors SALL4 and KLF5. Proc Natl Acad Sci U S A 2012;109:20584–9.
34. Tong D, Czerwenka K, Heinze G, Ryffel M, Schuster E, Witt A, et al. Expression of KLF5 is a prognostic factor for disease-free survival and overall survival in patients with breast cancer. Clin Cancer Res Off J Am Assoc Cancer Res 2006;12:2442–8.
35. Barretina J, Caponigro G, Stransky N, Venkatesan K, Margolin AA, Kim S, et al. The Cancer Cell Line Encyclopedia enables predictive modelling of anticancer drug sensitivity. Nature 2012;483:603–7.
36. The Cancer Genome Atlas Research Network. Comprehensive genomic characterization of head and neck squamous cell carcinomas. Nature 2015;517:576–82.
37. Layer RM, Chiang C, Quinlan AR, Hall IM. LUMPY: a probabilistic framework for structural variant discovery. Genome Biol 2014;15:R84.
38. Creyghton MP, Cheng AW, Welstead GG, Kooistra T, Carey BW, Steine EJ, et al. Histone H3K27ac separates active from poised enhancers and predicts developmental state. Proc Natl Acad Sci 2010;107:21931–6.
39. Hnisz D, Abraham BJ, Lee TI, Lau A, Saint-André V, Sigova AA, et al. Super-enhancers in the control of cell identity and disease. Cell 2013;155:934–47.
40. Lovén J, Hoke HA, Lin CY, Lau A, Orlando DA, Vakoc CR, et al. Selective inhibition of tumor oncogenes by disruption of super-enhancers. Cell 2013;153:320–34.
41. Whyte WA, Orlando DA, Hnisz D, Abraham BJ, Lin CY, Kagey MH, et al. Master transcription factors and mediator establish super-enhancers at key cell identity genes. Cell 2013;153:307–19.
42. Bailey SD, Zhang X, Desai K, Aid M, Corradin O, Cowper-Sal Lari R, et al. ZNF143 provides sequence specificity to secure chromatin interactions at gene promoters. Nat Commun 2015;2:6186.
43. Deng W, Lee J, Wang H, Miller J, Reik A, Gregory PD, et al. Controlling long-range genomic interactions at a native locus by targeted tethering of a looping factor. Cell 2012;149:1233–44.
44. Kagey MH, Newman JJ, Bilodeau S, Zhan Y, Orlando DA, van Berkum NL, et al. Mediator and cohesin connect gene expression and chromatin architecture. Nature 2010;467:430–5.
45. Dekker J, Mirny L. The 3D genome as moderator of chromosomal communication. Cell 2016;164:1110–21.
46. Dixon JR, Selvaraj S, Yue F, Kim A, Li Y, Shen Y, et al. Topological domains in mammalian genomes identified by analysis of chromatin interactions. Nature 2012;485:376–80.
47. Dixon JR, Jung I, Selvaraj S, Shen Y, Antosiewicz-Bourget JE, Lee AY, et al. Chromatin architecture reorganization during stem cell differentiation. Nature 2015;518:331–6.
48. Dowen JM, Fan ZP, Hnisz D, Ren G, Abraham BJ, Zhang LN, et al. Control of cell identity genes occurs in insulated neighborhoods in mammalian chromosomes. Cell 2014;159:374–87.
49. Rao SSP, Huntley MH, Durand NC, Stamenova EK, Bochkov ID, Robinson JT, et al. A 3D map of the human genome at kilobase resolution reveals principles of chromatin looping. Cell 2014;159:1665–80.
50. Hnisz D, Day DS, Young RA. Insulated neighborhoods: structural and functional units of mammalian gene control. Cell 2016;167:1188–200.
51. Hnisz D, Weintraub AS, Day DS, Valton A-L, Bak RO, Li CH, et al. Activation of proto-oncogenes by disruption of chromosome neighborhoods. Science 2016;351:1454–8.
52. Ooi WF, Xing M, Xu C, Yao X, Ramlee MK, Lim MC, et al. Epigenomic profiling of primary gastric adenocarcinoma reveals super-enhancer heterogeneity. Nat Commun 2016;7:12983.
53. Ojesina AI, Lichtenstein L, Freeman SS, Pedamallu CS, Imaz-Rosshandler I, Pugh TJ, et al. Landscape of genomic alterations in cervical carcinomas. Nature 2014;506:371–5.
54. The Cancer Genome Atlas Research Network. Integrated genomic characterization of oesophageal carcinoma. Nature 2017;541:169–75.
55. The Cancer Genome Atlas Research Network. Integrated genomic and molecular characterization of cervical cancer. Nature 2017;543:378–84.
56. Visel A, Blow MJ, Li Z, Zhang T, Akiyama JA, Holt A, et al. ChIP-seq accurately predicts tissue-specific activity of enhancers. Nature 2009;457:854–8.
57. Gilbert LA, Horlbeck MA, Adamson B, Villalta JE, Chen Y, Whitehead EH, et al. Genome-scale CRISPR-mediated control of gene repression and activation. Cell 2014;159:647–61.
58. Thakore PI, D'Ippolito AM, Song L, Safi A, Shivakumar NK, Kabadi AM, et al. Highly specific epigenome editing by CRISPR-Cas9 repressors for silencing of distal regulatory elements. Nat Methods 2015;12:1143–9.
59. Liu T, Ortiz JA, Taing L, Meyer CA, Lee B, Zhang Y, et al. Cistrome: an integrative platform for transcriptional regulation studies. Genome Biol 2011;12:R83.

60. Philipsen S, Suske G. A tale of three fingers: the family of mammalian Sp/XKLF transcription factors. Nucleic Acids Res 1999;27:2991–3000.
61. Turner J, Crossley M. Mammalian Krüppel-like transcription factors: more than just a pretty finger. Trends Biochem Sci 1999;24:236–40.
62. Zhang Z, Teng CT. Phosphorylation of Kruppel-like factor 5 (KLF5/IKLF) at the CBP interaction region enhances its transactivation function. Nucleic Acids Res 2003;31:2196–208.
63. Wang S, Sun H, Ma J, Zang C, Wang C, Wang J, et al. Target analysis by integration of transcriptome and ChIP-seq data with BETA. Nat Protoc 2013;8:2502–15.
64. The Cancer Genome Atlas Research Network, Weinstein JN, Collisson EA, Mills GB, Shaw KRM, Ozenberger BA, et al. The cancer genome atlas pan-cancer analysis project. Nat Genet 2013;45:1113–20.
65. Ciriello G, Miller ML, Aksoy BA, Senbabaoglu Y, Schultz N, Sander C. Emerging landscape of oncogenic signatures across human cancers. Nat Genet 2013;45:1127–33.
66. Lawrence MS, Stojanov P, Polak P, Kryukov GV, Cibulskis K, Sivachenko A, et al. Mutational heterogeneity in cancer and the search for new cancer-associated genes. Nature 2013;499:214–8.
67. Zack TI, Schumacher SE, Carter SL, Cherniack AD, Saksena G, Tabak B, et al. Pan-cancer patterns of somatic copy number alteration. Nat Genet 2013;45:1134–40.
68. Gao J, Aksoy BA, Dogrusoz U, Dresdner G, Gross B, Sumer SO, et al. Integrative analysis of complex cancer genomics and clinical profiles using the cBioPortal. Sci Signal 2013;6:pl1.
69. Cerami E, Gao J, Dogrusoz U, Gross BE, Sumer SO, Aksoy BA, et al. The cBio cancer genomics portal: an open platform for exploring multidimensional cancer genomics data. Cancer Discov 2012;2:401–4.
70. Liu N, Li H, Li S, Shen M, Xiao N, Chen Y, et al. The Fbw7/human CDC4 tumor suppressor targets proproliferative factor KLF5 for ubiquitination and degradation through multiple phosphodegron motifs. J Biol Chem 2010;285:18858–67.
71. Bialkowska AB, Liu Y, Nandan MO, Yang VW. A colon cancer-derived mutant of Krüppel-like factor 5 (KLF5) is resistant to degradation by glycogen synthase kinase 3β (GSK3β) and the E3 ubiquitin ligase F-box and WD repeat domain-containing 7α (FBW7α). J Biol Chem 2014;289:5997–6005.
72. Hao B, Oehlmann S, Sowa ME, Harper JW, Pavletich NP. Structure of a Fbw7-Skp1-cyclin E complex: multisite-phosphorylated substrate recognition by SCF ubiquitin ligases. Mol Cell 2007;26:131–43.
73. Orlicky S, Tang X, Willems A, Tyers M, Sicheri F. Structural basis for phosphodependent substrate selection and orientation by the SCFCdc4 ubiquitin ligase. Cell 2003;112:243–56.
74. O'Neil J, Grim J, Strack P, Rao S, Tibbitts D, Winter C, et al. FBW7 mutations in leukemic cells mediate NOTCH pathway activation and resistance to gamma-secretase inhibitors. J Exp Med 2007;204:1813–24.
75. Thompson BJ, Buonamici S, Sulis ML, Palomero T, Vilimas T, Basso G, et al. The SCFFBW7 ubiquitin ligase complex as a tumor suppressor in T cell leukemia. J Exp Med 2007;204:1825–35.
76. Liu Y, Olanrewaju YO, Zheng Y, Hashimoto H, Blumenthal RM, Zhang X, et al. Structural basis for Klf4 recognition of methylated DNA. Nucleic Acids Res 2014;42:4859–67.
77. Gudmundsson J, Sulem P, Gudbjartsson DF, Jonasson JG, Sigurdsson A, Bergthorsson JT, et al. Common variants on 9q22.33 and 14q13.3 predispose to thyroid cancer in European populations. Nat Genet 2009;41:460–4.
78. Clifton-Bligh RJ, Wentworth JM, Heinz P, Crisp MS, John R, Lazarus JH, et al. Mutation of the gene encoding human TTF-2 associated with thyroid agenesis, cleft palate and choanal atresia. Nat Genet 1998;19:399–401.
79. Revollo JR, Grimm AA, Imai S. The NAD biosynthesis pathway mediated by nicotinamide phosphoribosyltransferase regulates Sir2 activity in mammalian cells. J Biol Chem 2004;279:50754–63.
80. Shackelford RE, Mayhall K, Maxwell NM, Kandil E, Coppola D. Nicotinamide phosphoribosyltransferase in malignancy: a review. Genes Cancer 2013;4:447–56.
81. Wang B, Hasan MK, Alvarado E, Yuan H, Wu H, Chen WY. NAMPT overexpression in prostate cancer and its contribution to tumor cell survival and stress response. Oncogene 2011;30:907–21.
82. Aguirre AJ, Meyers RM, Weir BA, Vazquez F, Zhang C-Z, Ben-David U, et al. Genomic copy number dictates a gene-independent cell response to CRISPR/Cas9 targeting. Cancer Discov 2016;6:914–29.
83. Shin HY, Willi M, Yoo KH, Zeng X, Wang C, Metser G, et al. Hierarchy within the mammary STAT5-driven Wap super-enhancer. Nat Genet 2016;48:904–11.
84. Koepp DM, Schaefer LK, Ye X, Keyomarsi K, Chu C, Harper JW, et al. Phosphorylation-dependent ubiquitination of cyclin E by the SCFFbw7 ubiquitin ligase. Science 2001;294:173–7.
85. Oberg C, Li J, Pauley A, Wolf E, Gurney M, Lendahl U. The Notch intracellular domain is ubiquitinated and negatively regulated by the mammalian Sel-10 homolog. J Biol Chem 2001;276:35847–53.
86. Welcker M, Orian A, Jin J, Grim JE, Grim JA, Harper JW, et al. The Fbw7 tumor suppressor regulates glycogen synthase kinase 3 phosphorylation-dependent c-Myc protein degradation. Proc Natl Acad Sci U S A 2004;101:9085–90.
87. King B, Trimarchi T, Reavie L, Xu L, Mullenders J, Ntziachristos P, et al. The ubiquitin ligase FBXW7 modulates leukemia-initiating cell activity by regulating MYC stability. Cell 2013;153:1552–66.
88. Jaramillo MC, Zhang DD. The emerging role of the Nrf2–Keap1 signaling pathway in cancer. Genes Dev 2013;27:2179–91.
89. Clark VE, Harmancı AS, Bai H, Youngblood MW, Lee TI, Baranoski JF, et al. Recurrent somatic mutations in POLR2A define a distinct subset of meningiomas. Nat Genet 2016;48:1253–9.
90. Lawrence MS, Stojanov P, Mermel CH, Robinson JT, Garraway LA, Golub TR, et al. Discovery and saturation analysis of cancer genes across 21 tumour types. Nature 2014;505:495–501.
91. Zhu J, Sammons MA, Donahue G, Dou Z, Vedadi M, Getlik M, et al. Gain-of-function p53 mutants co-opt chromatin pathways to drive cancer growth. Nature 2015;525:206–11.
92. Barbieri CE, Baca SC, Lawrence MS, Demichelis F, Blattner M, Theurillat J-P, et al. Exome sequencing identifies recurrent SPOP, FOXA1 and MED12 mutations in prostate cancer. Nat Genet 2012;44:685–9.
93. Kamburov A, Lawrence MS, Polak P, Leshchiner I, Lage K, Golub TR, et al. Comprehensive assessment of cancer missense mutation clustering in protein structures. Proc Natl Acad Sci U S A 2015;112:E5486–5495.
94. Barrera LA, Vedenko A, Kurland JV, Rogers JM, Gisselbrecht SS, Rossin EJ, et al. Survey of variation in human transcription factors reveals prevalent DNA binding changes. Science 2016;351:1450–4.
95. Cheng THT, Thompson DJ, O'Mara TA, Painter JN, Glubb DM, Flach S, et al. Five endometrial cancer risk loci identified through genome-wide association analysis. Nat Genet 2016;48:667–74.
96. Childs EJ, Mocci E, Campa D, Bracci PM, Gallinger S, Goggins M, et al. Common variation at 2p13.3, 3q29, 7p13 and 17q25.1 associated with susceptibility to pancreatic cancer. Nat Genet 2015;47:911–6.
97. Petersen GM, Amundadottir L, Fuchs CS, Kraft P, Stolzenberg-Solomon RZ, Jacobs KB, et al. A genome-wide association study identifies pancreatic cancer susceptibility loci on chromosomes 13q22.1, 1q32.1 and 5p15.33. Nat Genet 2010;42:224–8.
98. Takata R, Akamatsu S, Kubo M, Takahashi A, Hosono N, Kawaguchi T, et al. Genome-wide association study identifies five new susceptibility loci for prostate cancer in the Japanese population. Nat Genet 2010;42:751–4.
99. Wolpin BM, Rizzato C, Kraft P, Kooperberg C, Petersen GM, Wang Z, et al. Genome-wide association study identifies multiple susceptibility loci for pancreatic cancer. Nat Genet 2014;46:994–1000.
100. Wu C, Miao X, Huang L, Che X, Jiang G, Yu D, et al. Genome-wide association study identifies five loci associated with susceptibility to pancreatic cancer in Chinese populations. Nat Genet 2011;44:62–6.
101. Grisanzio C, Freedman ML. Chromosome 8q24–associated cancers and MYC. Genes Cancer 2010;1:555–9.

102. Cowper-Sal·lari R, Zhang X, Wright JB, Bailey SD, Cole MD, Eeckhoute J, et al. Breast cancer risk-associated SNPs modulate the affinity of chromatin for FOXA1 and alter gene expression. Nat Genet 2012;44:1191–8.
103. Pomerantz MM, Ahmadiyeh N, Jia L, Herman P, Verzi MP, Doddapaneni H, et al. The 8q24 cancer risk variant rs6983267 shows long-range interaction with MYC in colorectal cancer. Nat Genet 2009;41:882–4.
104. Wright JB, Brown SJ, Cole MD. Upregulation of c-MYC in cis through a large chromatin loop linked to a cancer risk-associated single-nucleotide polymorphism in colorectal cancer cells. Mol Cell Biol 2010;30:1411–20.
105. Zhang X, Cowper-Sal lari R, Bailey SD, Moore JH, Lupien M. Integrative functional genomics identifies an enhancer looping to the SOX9 gene disrupted by the 17q24.3 prostate cancer risk locus. Genome Res 2012;22:1437–46.
106. Zhang X, Bailey SD, Lupien M. Laying a solid foundation for Manhattan 'Setting the functional basis for the post-GWAS era.' Trends Genet TIG 2014;30:140–9.
107. Zhao D, Zhi X, Zhou Z, Chen C. TAZ antagonizes the WWP1-mediated KLF5 degradation and promotes breast cell proliferation and tumorigenesis. Carcinogenesis 2012;33:59–67.
108. Gao Y, Wu K, Chen Y, Zhou J, Du C, Shi Q, et al. Beyond proliferation: KLF5 promotes angiogenesis of bladder cancer through directly regulating VEGFA transcription. Oncotarget 2015;6:43791–805.
109. Mermel CH, Schumacher SE, Hill B, Meyerson ML, Beroukhim R, Getz G. GISTIC2.0 facilitates sensitive and confident localization of the targets of focal somatic copy-number alteration in human cancers. Genome Biol 2011;12:R41.
110. Li H, Durbin R. Fast and accurate short read alignment with Burrows-Wheeler transform. Bioinforma Oxf Engl 2009;25:1754–60.
111. Zhang Y, Liu T, Meyer CA, Eeckhoute J, Johnson DS, Bernstein BE, et al. Model-based analysis of ChIP-Seq (MACS). Genome Biol 2008;9:R137.
112. Thurman RE, Rynes E, Humbert R, Vierstra J, Maurano MT, Haugen E, et al. The accessible chromatin landscape of the human genome. Nature 2012;489:75–82.
113. Quinlan AR, Hall IM. BEDTools: a flexible suite of utilities for comparing genomic features. Bioinforma Oxf Engl 2010;26:841–2.
114. Nikolayeva O, Robinson MD. edgeR for differential RNA-seq and ChIP-seq analysis: an application to stem cell biology. Methods Mol Biol Clifton NJ 2014;1150:45–79.
115. Robinson MD, McCarthy DJ, Smyth GK. edgeR: a Bioconductor package for differential expression analysis of digital gene expression data. Bioinforma Oxf Engl 2010;26:139–40.
116. Li H, Handsaker B, Wysoker A, Fennell T, Ruan J, Homer N, et al. The sequence alignment/map format and SAMtools. Bioinforma Oxf Engl 2009;25:2078–9.
117. Doench JG, Fusi N, Sullender M, Hegde M, Vaimberg EW, Donovan KF, et al. Optimized sgRNA design to maximize activity and minimize off-target effects of CRISPR-Cas9. Nat Biotechnol 2016;34:184–91.
118. Sanjana NE, Shalem O, Zhang F. Improved vectors and genome-wide libraries for CRISPR screening. Nat Methods 2014;11:783–4.
119. Dobin A, Davis CA, Schlesinger F, Drenkow J, Zaleski C, Jha S, et al. STAR: ultrafast universal RNA-seq aligner. Bioinforma Oxf Engl 2013;29:15–21.
120. Li B, Dewey CN. RSEM: accurate transcript quantification from RNA-Seq data with or without a reference genome. BMC Bioinformatics 2011;12:323.
121. Ritchie ME, Phipson B, Wu D, Hu Y, Law CW, Shi W, et al. limma powers differential expression analyses for RNA-sequencing and microarray studies. Nucleic Acids Res 2015;43:e47.
122. Shao DD, Tsherniak A, Gopal S, Weir BA, Tamayo P, Stransky N, et al. ATARiS: Computational quantification of gene suppression phenotypes from multisample RNAi screens. Genome Res 2013;23:665–78.